

Bethe Ansatz solution of triangular trimers on the triangular lattice

Alain Verberkmoes and Bernard Nienhuis
*Instituut voor Theoretische Fysica, Valckenierstraat 65,
 1018 XE Amsterdam, The Netherlands*

September 4, 1999

Abstract

Details are presented of a recently announced exact solution of a model consisting of triangular trimers covering the triangular lattice. The solution involves a coordinate Bethe Ansatz with two kinds of particles. It is similar to that of the square–triangle random tiling model, due to M. Widom and P. A. Kalugin. The connection of the trimer model with related solvable models is discussed.

1 Introduction

The dimer problem is one of the classic models of statistical mechanics. A dimer in this context is a particle that occupies two neighbouring sites of a lattice. In the dimer–monomer model dimers and monomers (particles occupying one lattice site each) are placed on a lattice such that they cover all sites, without overlap. Equivalently the monomers can be viewed as empty sites; the lattice is then partly covered with dimers. This model was introduced to describe diatomic molecules adsorbed on a substrate [1]. Attempts have been made in vain to solve this model exactly, that is, to calculate its free energy. The special case that there are no empty sites (monomers) is known as the dimer problem. There the dimers cover the lattice completely and without overlap. This model has been solved for planar lattices, independently by Kasteleyn [2] and by Temperley and Fisher [3]. Their solution is based on the possibility to express the partition function of the model as a Pfaffian. For many planar lattices the dimer problem can also be solved by means of the Bethe Ansatz. On the honeycomb lattice for example it can be formulated as a five-vertex model. This is a special case of the six-vertex model, whose Bethe Ansatz solution is well-known [4–11]. A review of the dimer problem is given in [12].

Inspired by the solvability of the dimer model, we consider lattice coverings by trimers. A trimer is a particle that occupies three lattice sites. We only consider triangular trimers, which live naturally on the triangular lattice. As in the dimer model, we require that these particles cover the lattice completely and without overlap. Thus every lattice site is covered by precisely one trimer. Figure 1 shows a typical configuration.

As will be shown in Subsection 2.2 this model has a structure of domains separated by domain walls. The domains are hexagonal, and the domain walls form a honeycomb network. Similar domain wall structures are used to describe an incommensurate phase of a monolayer of a monoatomic gas adsorbed on a hexagonal substrate [13]. The entropy of such a network is largely due to the “breathing” of the cells: it is possible to blow up a domain and simultaneously shrink its six neighbours, or vice versa.

Hexagonal domain wall structures also occur in the square–triangle random tiling model [14]. For that model a coordinate Bethe Ansatz was found by Widom [15]. The resulting Bethe Ansatz equations were solved analytically in the thermodynamic limit by Kalugin [16]. An exact solution of the trimer model was announced in [17]; in the present paper we describe its the derivation.

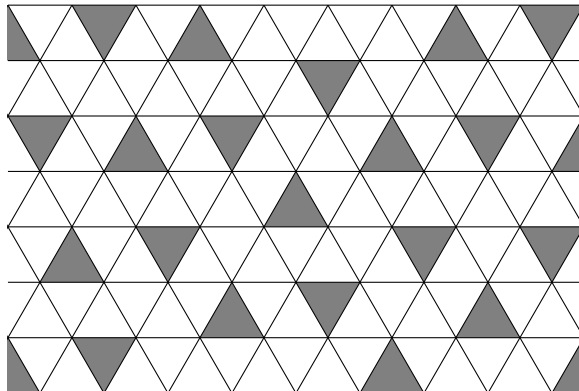


Figure 1: A typical configuration of the trimer model. Each lattice site belongs to precisely one trimer.

The solution is very similar to that for the square–triangle tiling, and we closely follow Kalugin’s arguments. The outline of our calculation is as follows. A transfer matrix for the model is formulated. After the choice of a reference state two types of elementary excitations are found. They are closely related to the above-mentioned domain wall structure of the model. In order to diagonalise the transfer matrix a coordinate Bethe Ansatz is set up in terms of the elementary excitations. The resulting semi-grand canonical ensemble is discussed. In the thermodynamic limit the Bethe Ansatz leads to a set of two coupled integral equations. These can be solved in a special case. From their solution the relevant physical quantities are computed. The results of the calculation are summarised in Subsection 6.5. We then consider the entropy as function of the density of down trimers. The model undergoes two phase transitions in the density of down trimers.

Finally we discuss the relation between the trimer model, the square–triangle random tiling model, and yet another solvable model with a hexagonal domain wall structure.

2 Preliminaries

2.1 Sub-lattices

Figure 2 shows a very regular configuration of the model, in which the trimers are positioned on a sub-lattice of the triangular faces. There are six such sub-lattices, which we number $0, 1, \dots, 5$ as indicated in the figure. Note that the even-numbered sub-lattices consist of the up triangles while the down triangles constitute the odd-numbered sub-lattices. For a given configuration let N denote the total number of trimers and let N_i denote the number of trimers on sub-lattice i . We wish to compute the entropy per trimer as a function of the sub-lattice densities

$$\rho_0 = \frac{N_0}{N}, \quad \rho_1 = \frac{N_1}{N}, \quad \dots, \quad \rho_5 = \frac{N_5}{N}.$$

These densities satisfy the obvious linear constraint

$$\rho_0 + \rho_1 + \rho_2 + \rho_3 + \rho_4 + \rho_5 = 1. \quad (1)$$

In Subsection 2.5 it will be shown that when toroidal boundary conditions are imposed the densities also satisfy a quadratic constraint:

$$\rho_0\rho_2 + \rho_2\rho_4 + \rho_4\rho_0 = \rho_1\rho_5 + \rho_3\rho_5 + \rho_5\rho_1. \quad (2)$$

Hence of the six sub-lattice densities only four are independent. In order to be able to set up a transfer matrix we pass to the grand canonical ensemble. The trimers on each sub-lattice i are

given a fugacity $w_i = \exp(\mu_i)$. After the transfer matrix has been diagonalised we shall Legendre transform back to the canonical ensemble.

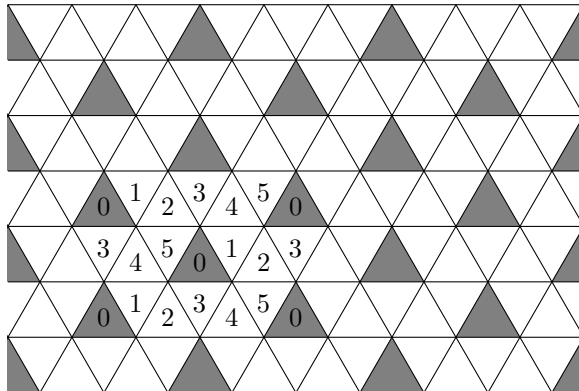


Figure 2: A regular configuration in which the trimers occupy a sub-lattice of the faces. There are six such sub-lattices, numbered $0, 1, \dots, 5$.

2.2 Domains and walls

Occupying sub-lattice 0 completely while leaving the other five sub-lattices empty results in the configuration of the model shown in Figure 2. This arrangement does not admit local changes. However, it is possible to flip a whole line of trimers. Such a line can be viewed as a wall separating two domains consisting of trimers on sub-lattice 0. These domain walls come in three types (orientations), corresponding to the three odd-numbered sub-lattices. When two walls of different type meet a wall of the third type is formed. A trimer on sub-lattice 2 or 4 occurs when three domain walls of different type meet in a Y, but this does not happen at an upside-down Y. Figure 3 show examples of how the three types of domain walls can meet. In a general configuration the domain walls form a hexagonal network.

2.3 Transfer matrix

In an allowed configuration of the model each lattice site belongs to precisely one trimer. This trimer sits either on one of the three lattice faces above the site or on one of the three faces below the site. Label the site with a “spin” \uparrow or \downarrow accordingly.

Consider a horizontal row of lattice sites and assume that the trimer configuration below that row is given. It determines the spins on that row. The sites occupied by a trimer below have a spin \downarrow , while those not occupied by such a trimer must needs carry a spin \uparrow . Now consider the next layer of lattice faces, above this row. In order to decide what trimer configurations on this layer are possible, it is sufficient to know which sites are already covered. This is precisely the information encoded by the spins.

This shows that the model can be described in terms of a transfer matrix that connects two consecutive rows of spins. Let σ denote be the spin configuration on the lower row and τ the spin configurations on the upper row. Consider all trimer arrangements (without overlaps) on the layer in between that are compatible with the spin configurations σ and τ . (Generally there is at most one such arrangement.) The sum of their Boltzmann weights is the transfer matrix element $T_{\tau\sigma}$.

The rows of lattice sites in the model come in two types, call them A and B, that are shifted with respect to each other. The rows of type A and B alternate. Hence there are in fact two transfer matrices, T_{AB} for layers with upper row of type A and lower row of type B, and T_{BA} for layers with upper row of type B and lower row of type A. The products $T_{AB}T_{BA}$ and $T_{BA}T_{AB}$ are double transfer matrices that act between rows of equal type. Take a lattice consisting of $2M$

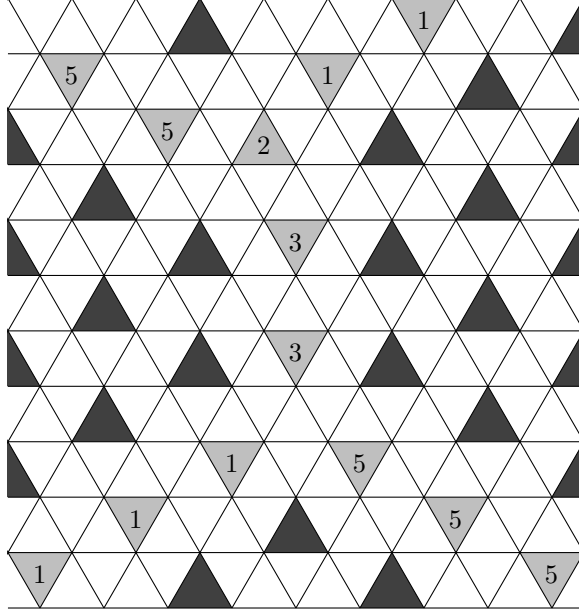


Figure 3: The configuration from Figure 2 admits line excitations. These domain walls can meet in Ys (top) and upside-down Ys (bottom). The Ys are chiral; the mirror image of the Y shown here contains a trimer on sub-lattice 4 instead of 2. The upside-down Ys are achiral. To guide the eye the trimers not on sub-lattice 0 are shaded lighter; the numbers indicate their sub-lattices.

layers and impose periodic boundary conditions in the vertical direction, that is, identify the lower and upper row. As usual the partition function of the model on this lattice is

$$Z = \text{Tr} (T_{AB}T_{BA})^M = \text{Tr} (T_{BA}T_{AB})^M.$$

In the limit that M tends to infinity the partition sum is dominated by the largest eigenvalue of $T_{AB}T_{BA}$ or $T_{BA}T_{AB}$.

The matrices T_{AB} and T_{BA} can be combined into a single matrix

$$T = \begin{pmatrix} 0 & T_{AB} \\ T_{BA} & 0 \end{pmatrix}$$

acting on vectors

$$\psi = \begin{pmatrix} \psi_A \\ \psi_B \end{pmatrix}$$

where ψ_A and ψ_B are “wave functions” on the rows of type A and B, respectively. If such a vector is an eigenvector of T with eigenvalue Λ then ψ_A and ψ_B are eigenvectors of $T_{AB}T_{BA}$ and $T_{BA}T_{AB}$, respectively, with eigenvalue Λ^2 .

Some identification of the row types A and B could have been chosen in order to avoid the complication discussed. This amounts to skewing the lattice or, equivalently, the transfer matrix direction. Because it breaks a mirror symmetry of the system we have avoided this solution.

2.4 Conserved quantities and elementary excitations

In the configuration obtained by fully occupying sub-lattice 0, each row of spins consists of repeating blocks $\uparrow\downarrow\uparrow$. Therefore we group the sites into blocks of three, as in Figure 4. Number the blocks in a row from the left to the right.

A row of spins with $n_{\downarrow\bullet\bullet} + n_{\bullet\uparrow\bullet} = 1$ and $n_{\bullet\bullet\downarrow} + n_{\bullet\uparrow\bullet} = 0$ is obtained by replacing one block, say at position x , in the reference state with $\downarrow\downarrow\uparrow$. There is only one possible configuration of trimers on the layer above, see Figure 5. The row above consists of blocks $\uparrow\downarrow\uparrow$ except for one block $\downarrow\downarrow\uparrow$ at position $x - \frac{1}{2}$. Thus the transfer matrix has shifted the block $\downarrow\downarrow\uparrow$ in the lower row half a step to the left in the upper row. This block is a left-moving elementary excitation of the reference state. It will be called an L-particle. Similarly the block $\uparrow\downarrow\downarrow$ is an elementary right-moving excitation, or R-particle. The conserved quantities $n_{\downarrow\bullet\bullet} + n_{\bullet\uparrow\bullet}$ and $n_{\bullet\bullet\downarrow} + n_{\bullet\uparrow\bullet}$ are the number n_L of L-particles and the number n_R of R-particles, respectively.

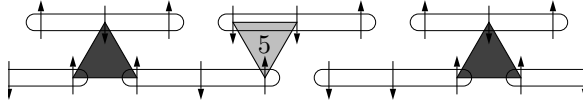


Figure 5: There is only one way to fit trimers below a row consisting of one block $\downarrow\downarrow\uparrow$ amidst blocks $\uparrow\downarrow\uparrow$. It leads to another such row of spins below.

The particle content of the blocks $\uparrow\downarrow\uparrow$, $\downarrow\downarrow\uparrow$ and $\uparrow\downarrow\downarrow$ has now been determined. For each of the other five blocks both n_L and n_R are greater than zero. Therefore these blocks are combinations of the elementary excitations. They will be discussed in more detail in Subsections 3.3–3.5.

We have found no other conserved quantities than n_L and n_R (except in the special case when $n_L = 0$ or $n_R = 0$).

2.5 World lines and quadratic constraint

Divide the lattice into hexagonal patches containing one face from each sub-lattice, in such a way that the lower middle triangle of each patch belongs to sub-lattice 0. There are six trimer configurations possible on such a patch. Decorate each patch according to this configuration as shown in Figure 6. It is tedious but straightforward to verify that the decorations of the patches making up the lattice fit together, giving a set of solid and dashed lines running from the bottom to the top of the lattice. It can also be checked that the crossings of these lines with the lattice rows correspond to the locations of the L-particles (solid lines) and R-particles (dashed lines). Hence these lines are the “world lines” of the L-particles and R-particles where the horizontal and vertical lattice direction are viewed as “space” and “time” respectively.

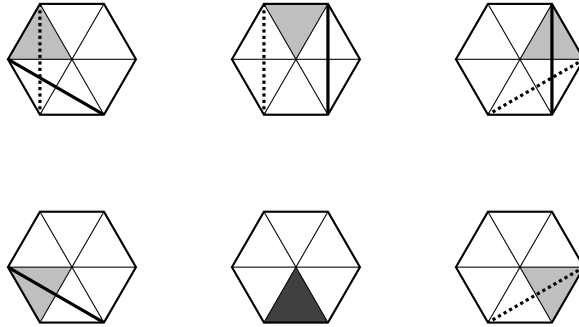


Figure 6: Decompose the triangular lattice into hexagonal patches such that the lower middle triangle of each patch belongs to sub-lattice 0. The other triangles, in counterclockwise order, then belong to sub-lattice 1, 4, 3, 2 and 5. These patches can be decorated with the world lines of the L-particles (solid) and R-particles (dashed).

Impose toroidal boundary conditions. We now derive the quadratic constraint (2) by the same method as that used for rectangle–triangle random tiling models in [18] and [19]. Cut the torus

open along a horizontal row of sites, so that the model is now on a cylinder. By stacking a number of copies of the configuration on top of each other we can achieve that each world line winds around the cylinder an integer number of times. Let $2M$ be the number of rows. In each row we can count the number of L-particles and R-particles:

$$\begin{aligned} n_L &= L - n_0 - n_1 + n_3 + n_4, \\ n_R &= L - n_0 + n_2 + n_3 - n_5. \end{aligned}$$

Summing over the entire lattice yields

$$2Mn_L = 2LM - N_0 - N_1 + N_3 + N_4, \quad (7)$$

$$2Mn_R = 2LM - N_0 + N_2 + N_3 - N_5. \quad (8)$$

Since the world lines of the L-particles do not cross each other, they all have the same winding number W_L . In order to compute this winding number consider the total leftward movement of the L-particles. There are n_L such particles, each of them winds around the cylinder W_L times, and each winding constitutes a movement of L blocks to the left, so the total leftward movement amounts $n_L W_L L$ blocks. It can be seen from Figure 6 that an L-particle moves half a block to the left at a trimer on sub-lattice 2 or 5, while there is no horizontal movement of L-particles at a trimer on another sub-lattice. Summing over the entire lattice shows the total leftward movement of the L-particles to be $\frac{1}{2}(N_2 + N_5)$ blocks. Hence

$$n_L W_L L = \frac{1}{2} (N_2 + N_5). \quad (9)$$

Fully analogously one has

$$n_R W_R L = \frac{1}{2} (N_1 + N_4). \quad (10)$$

Now consider the number of crossings of L-particle lines and R-particle lines. There are n_L L-particles each winding leftward around the cylinder W_L times, and n_R R-particles each winding rightward around the cylinder W_R times, so the number of crossings is $n_L n_R (W_L + W_R)$. From Figure 6 it is seen that crossings occur precisely at trimers on sub-lattice 2 or 4, so that the number of crossings is $N_2 + N_4$. Equating these two expressions for the number of crossings gives

$$n_L n_R (W_L + W_R) = N_2 + N_4.$$

Substituting into the above equation first (9) and (10), then (7) and (8), then multiplying by $2LM$ and finally using

$$2LM = N_0 + N_1 + N_2 + N_3 + N_4 + N_5$$

yields

$$N_1 N_3 + N_3 N_5 + N_5 N_1 = N_0 N_2 + N_2 N_4 + N_4 N_0.$$

Dividing by N^2 gives (2). For the sake of the argument we have stacked a number of copies of the original configuration on top of each other, but the resulting (2) is not affected by this.

3 Bethe Ansatz

In this section we describe a Bethe Ansatz (BA) that diagonalises the transfer matrix. Since the particle numbers n_L and n_R are conserved quantities the transfer matrix is block diagonal. We begin by considering the sector with $n_L = 0$ and $n_R = 0$ and then pass to sectors with higher particle numbers.

3.1 No particles

The only state in the sector $n_L = 0, n_R = 0$ is the reference state which consists entirely of blocks $\uparrow\downarrow\uparrow$, so this sector is one-dimensional. Therefore the transfer matrix acting on this sector is trivially diagonal. The layer between two consecutive rows in the reference state consists of L trimers on sub-lattice 0, so its Boltzmann weight is w_0^L . It is the eigenvalue of the transfer matrix in this sector. For convenience we define the “reduced” transfer matrix \tilde{T} to be the transfer matrix T divided by w_0^L .

3.2 One L-particle

Consider a row of spins containing a single L-particle ($\downarrow\downarrow\uparrow$) at position x . The transfer matrix has shifted this particle from position $x + \frac{1}{2}$ in the row below half a step to the left, see Figure 5. The layer between the two rows contains $L - 1$ trimers on sub-lattice 0 and one trimer on sub-lattice 5. Hence the action of the (reduced) transfer matrix on the “wave function” is given by

$$(\tilde{T}\psi)(\downarrow\downarrow\uparrow x) = \frac{w_5}{w_0}\psi(\downarrow\downarrow\uparrow x + \frac{1}{2}).$$

(We use $\downarrow\downarrow\uparrow x$ as notation for the row configuration that has a block $\downarrow\downarrow\uparrow$ at position x and blocks $\uparrow\downarrow\uparrow$ at the other positions.) The solution of the eigenvalue problem $\tilde{T}\psi = \tilde{\Lambda}\psi$ is

$$\psi(\downarrow\downarrow\uparrow x) = A_u u^x,$$

where A_u is some constant, and

$$\tilde{\Lambda} = \frac{w_5}{w_0} u^{\frac{1}{2}}.$$

3.3 One L-particle and one R-particle

Consider a row of spins containing an L-particle ($\downarrow\downarrow\uparrow$) at position x and an R-particle ($\uparrow\downarrow\downarrow$) at position y , with $x < y$. If the particles are apart, this situation was formed by shifting the L-particle to the left and the R-particle to the right:

$$(\tilde{T}\psi)(\downarrow\downarrow\uparrow x, \uparrow\downarrow\downarrow y) = \frac{w_5 w_1}{w_0^2} \psi(\downarrow\downarrow\uparrow x + \frac{1}{2}, \uparrow\downarrow\downarrow y - \frac{1}{2}) \quad \text{if } y - x > 1. \quad (11)$$

(We write the arguments of ψ in order of increasing position; for example, the notation in the LHS of (11) implies that $x < y$.) If however the particles are next to each other, the situation was formed from a “bound state” ($\downarrow\downarrow\downarrow$), see Figure 3 (top):

$$(\tilde{T}\psi)(\downarrow\downarrow\uparrow z - \frac{1}{2}, \uparrow\downarrow\downarrow z + \frac{1}{2}) = \frac{w_5 w_1}{w_0^2} \psi(\downarrow\downarrow\downarrow z). \quad (12)$$

This bound state was formed from another type of bound state ($\uparrow\uparrow\uparrow$):

$$(\tilde{T}\psi)(\downarrow\downarrow\downarrow z) = \frac{w_4 w_1}{w_0} \psi(\uparrow\uparrow\uparrow z - \frac{1}{2}) + \frac{w_5 w_2}{w_0} \psi(\uparrow\uparrow\uparrow z + \frac{1}{2}). \quad (13)$$

The two terms correspond to two chiral configurations one of which is depicted in Figure 3. This bound state was formed from an R-particle and an L-particle next to each other, the R-particle sitting to the left of the L-particle:

$$(\tilde{T}\psi)(\uparrow\uparrow\uparrow z) = \frac{1}{w_0} \psi(\uparrow\downarrow\downarrow z - \frac{1}{2}, \downarrow\downarrow\uparrow z + \frac{1}{2}). \quad (14)$$

This configuration can have arisen from the same bound state again. The alternation of this bound state and the situation where the R-particle and L-particle are next to each other ($\uparrow\downarrow\downarrow \downarrow\downarrow\uparrow$) corresponds to the vertical domain wall in Figure 3. The configuration where the particles are

next to each other can also have arisen by shifting the R-particle half a step to the right and the L-particle half a step to the left, see Figure 3 (bottom):

$$(\tilde{T}\psi)(\uparrow\downarrow\downarrow z - \frac{1}{2}, \downarrow\downarrow\uparrow z + \frac{1}{2}) = w_3\psi(\uparrow\uparrow\uparrow z) + \frac{w_1w_5}{w_0^2}\psi(\uparrow\downarrow\downarrow z - 1, \downarrow\downarrow\uparrow z + 1). \quad (15)$$

Finally, a configuration where the particles are apart was formed by shifting the R-particle half a step to the right and the L-particle half a step to the left:

$$(\tilde{T}\psi)(\uparrow\downarrow\downarrow y, \downarrow\downarrow\uparrow x) = \frac{w_1w_5}{w_0^2}\psi(\uparrow\downarrow\downarrow y - \frac{1}{2}, \downarrow\downarrow\uparrow x + \frac{1}{2}) \quad \text{if } x - y > 1. \quad (16)$$

We want to solve the eigenvalue equation $\tilde{T}\psi = \tilde{\Lambda}\psi$ for (11)–(16). The eigenvalue equation for (11) and (12) is satisfied by

$$\begin{aligned} \psi(\downarrow\downarrow\uparrow x, \uparrow\downarrow\downarrow y) &= A_{uv}u^xv^y, \\ \psi(\downarrow\downarrow\downarrow z) &= A_{uv}u^zv^z \end{aligned}$$

with eigenvalue

$$\tilde{\Lambda} = \frac{w_5}{w_0}u^{\frac{1}{2}}\frac{w_1}{w_0}v^{-\frac{1}{2}}.$$

Similarly the eigenvalue equation for (14), (15), and (16), with the same value for $\tilde{\Lambda}$, is satisfied by

$$\begin{aligned} \psi(\uparrow\downarrow\downarrow y, \downarrow\downarrow\uparrow x) &= A_{vu}v^yu^x \quad \text{if } x - y > 1, \\ \psi(\uparrow\downarrow\downarrow z - \frac{1}{2}, \downarrow\downarrow\uparrow z + \frac{1}{2}) &= B_{vu}A_{vu}v^{z-\frac{1}{2}}u^{z+\frac{1}{2}}, \\ \psi(\uparrow\uparrow\uparrow z) &= DB_{vu}A_{vu}v^zu^z, \end{aligned}$$

where

$$B_{vu} = \left(1 - \frac{w_0^3w_3}{w_1^2w_5^2}u^{-1}v\right)^{-1}, \quad (17)$$

$$D = \frac{w_0}{w_1w_5}. \quad (18)$$

The eigenvalue equation for (13) is satisfied too if

$$\frac{A_{uv}}{A_{vu}} = S_{uv},$$

where

$$S_{uv} = \frac{w_0^2}{w_1w_5} \left(\frac{w_4}{w_5}u^{-1} + \frac{w_2}{w_1}v \right) \left(1 - \frac{w_0^3w_3}{w_1^2w_5^2}u^{-1}v \right)^{-1}. \quad (19)$$

The above analysis suggests to interpret the bound state $\downarrow\downarrow\downarrow$ as LR (in that order) and the bound state $\uparrow\uparrow\uparrow$ as RL. The eigenfunction is then written

$$\begin{aligned} \psi(\text{L } x, \text{R } y) &= A_{uv}u^xv^y, \\ \psi(\text{R } y, \text{L } x) &= \begin{cases} A_{vu}v^yu^x & \text{if } x - y \geq 2, \\ B_{vu}A_{vu}v^yu^x & \text{if } x - y = 1, \\ DB_{vu}A_{vu}v^yu^x & \text{if } x - y = 0. \end{cases} \end{aligned}$$

3.4 Two L-particles and one R-particle

A similar but more tedious analysis can be carried out for the sector with two L-particles and one R-particle. There is a new bound state ($\downarrow\uparrow\uparrow$) that can be interpreted as LRL. A solution of the eigenvalue problem $\tilde{T}\psi = \tilde{\Lambda}\psi$ is given by

$$\begin{aligned} \psi(\text{L } x_1, \text{L } x_2, \text{R } y) &= \sum_{\pi} A_{u_{\pi(1)}u_{\pi(2)}v} u_{\pi(1)}^{x_1} u_{\pi(2)}^{x_2} v^y, \\ \psi(\text{L } x_1, \text{R } y, \text{L } x_2) &= \begin{cases} \sum_{\pi} A_{u_{\pi(1)}vu_{\pi(2)}} u_{\pi(1)}^{x_1} v^y u_{\pi(2)}^{x_2} & \text{if } x_2 - y \geq 2, \\ \sum_{\pi} B_{vu_{\pi(2)}} A_{u_{\pi(1)}vu_{\pi(2)}} u_{\pi(1)}^{x_1} v^y u_{\pi(2)}^{x_2} & \text{if } x_2 - y = 1, \\ \sum_{\pi} DB_{vu_{\pi(2)}} A_{u_{\pi(1)}vu_{\pi(2)}} u_{\pi(1)}^{x_1} v^y u_{\pi(2)}^{x_2} & \text{if } x_2 - y = 0, \end{cases} \\ \psi(\text{R } y, \text{L } x_1, \text{L } x_2) &= \begin{cases} \sum_{\pi} A_{vu_{\pi(1)}u_{\pi(2)}} v^y u_{\pi(1)}^{x_1} u_{\pi(2)}^{x_2} & \text{if } x_1 - y \geq 2, \\ \sum_{\pi} B_{vu_{\pi(1)}} A_{vu_{\pi(1)}u_{\pi(2)}} v^y u_{\pi(1)}^{x_1} u_{\pi(2)}^{x_2} & \text{if } x_1 - y = 1, \\ \sum_{\pi} DB_{vu_{\pi(1)}} A_{vu_{\pi(1)}u_{\pi(2)}} v^y u_{\pi(1)}^{x_1} u_{\pi(2)}^{x_2} & \text{if } x_1 - y = 0, \end{cases} \end{aligned}$$

where π runs through the permutations of $\{1, 2\}$. The amplitudes must satisfy

$$\frac{A_{u_i u_{i'} v}}{A_{u_{i'} u_i v}} = \frac{A_{v u_i u_{i'}}}{A_{v u_{i'} u_i}} = -1 \quad (i \neq i'), \quad (20)$$

$$\frac{A_{u_i v u_{i'}}}{A_{v u_i u_{i'}}} = \frac{A_{u_{i'} u_i v}}{A_{u_{i'} v u_i}} = S_{u_i v} \quad (i \neq i'), \quad (21)$$

with $S_{u_i v}$ given by (19). Note that the amplitude ratio in (20) does not depend on v and that the amplitude ratio in (21) does not depend on $u_{i'}$. The eigenvalue is given by

$$\tilde{\Lambda} = \frac{w_5}{w_0} u_1^{\frac{1}{2}} \frac{w_5}{w_0} u_2^{\frac{1}{2}} \frac{w_1}{w_0} v^{-\frac{1}{2}}.$$

3.5 Arbitrary particle numbers

With two L-particles and two R-particles, there is a new bound state ($\downarrow\uparrow\downarrow$) that can be interpreted as LRLR. This completes the list of possible blocks and their interpretation in terms of particles, see Table 1.

Table 1: The three-spin blocks.

spins	particles
$\uparrow\downarrow\uparrow$	none
$\downarrow\downarrow\uparrow$	L
$\uparrow\downarrow\downarrow$	R
$\downarrow\downarrow\downarrow$	LR
$\uparrow\uparrow\uparrow$	RL
$\downarrow\uparrow\uparrow$	LRL
$\uparrow\uparrow\downarrow$	RLR
$\downarrow\uparrow\downarrow$	LRLR

The solution given above of the eigenvalue problem $\tilde{T}\psi = \tilde{\Lambda}\psi$ for two L-particles and one R-particle generalises to the higher sectors. Before describing this generalisation we introduce a notational convention. The index i , running from 1 to n_L , will be used to number L-particle positions and Bethe Ansatz. The index j , between 1 and n_R , will refer to R-particles. Now consider a succession of L-particles with coordinates $x_1 \leq x_2 \leq \dots \leq x_{n_L}$ and R-particles with

coordinates $y_1 \leq y_2 \leq \dots \leq y_{n_R}$. (Note that $x_i = x_{i+1}$ can arise only from a block LRL or LRLR, so $x_i = y_j = x_{i+1}$ for some y_j .) The value of the wave function is given by

$$\psi(\text{particle sequence}) = \sum_{\pi} \sum_{\sigma} \prod (D \text{ and } B \dots) A \dots \prod \left(u_{\pi(i)}^{x_i} \text{ and } v_{\sigma(j)}^{y_j} \right), \quad (22)$$

where π and σ run through all permutations of $\{1, 2, \dots, n_L\}$ and $\{1, 2, \dots, n_R\}$, respectively. We shall now describe the factors in the RHS of (22). For each segment R y_j , L x_i in the particle sequence with $x_i - y_j = 1$ there is a factor $B_{v_{\sigma(j)} u_{\pi(i)}}$. For each such segment with $x_i - y_j = 0$ there is a factor $DB_{v_{\sigma(j)} u_{\pi(i)}}$. The amplitude $A \dots$ depends on the sequence of the variables u and v corresponding to the sequence of L-particles and R-particles. The u are in the order $u_{\pi(1)}, u_{\pi(2)}, \dots, u_{\pi(n_L)}$ and the v are in the order $v_{\sigma(1)}, v_{\sigma(2)}, \dots, v_{\sigma(n_R)}$, but the two sequences interlace. The amplitudes $A \dots$ are defined up to an overall factor by the conditions

$$\begin{aligned} \frac{A \dots u_i u_{i'} \dots}{A \dots u_{i'} u_i \dots} &= -1 \quad (i \neq i'), \\ \frac{A \dots v_j v_{j'} \dots}{A \dots v_{j'} v_j \dots} &= -1 \quad (j \neq j'), \\ \frac{A \dots u_i v_j \dots}{A \dots v_j u_i \dots} &= S_{u_i v_j} \end{aligned}$$

with $S_{u_i v_j}$ given by (19). Finally comes the product of all the $u_{\pi(i)}^{x_i}$ and $v_{\sigma(j)}^{y_j}$. The eigenvalue for the eigenfunction ψ is given by

$$\tilde{\Lambda} = \prod_{i=1}^{n_L} \frac{w_5}{w_0} u_i^{\frac{1}{2}} \prod_{j=1}^{n_R} \frac{w_1}{w_0} v_j^{-\frac{1}{2}}. \quad (23)$$

We have no rigorous proof that the above solution is correct for all sectors, but using computer algebra we have verified it for $n_L + n_R \leq 5$.

It should be noted that the formulation of the solution depends on the particle interpretation of the three-spin blocks. The particle content of each three-spin block is determined by $n_L = n_{\downarrow\bullet\bullet} + n_{\bullet\uparrow\bullet}$ and $n_R = n_{\bullet\bullet\downarrow} + n_{\bullet\uparrow\bullet}$, but the order of the particles within a block can be chosen. For example, we could interpret $\downarrow\uparrow\uparrow$ as LLR, LRL or RLL. The choices in Table 1 lead to a simple description of the eigenfunctions; each factor D or B depends only on two successive particles. Other choices than those in Table 1 would make the formulation of the eigenfunctions more awkward; there would be more factors than just D and B , and some would depend on non-successive particles.

3.6 Bethe Ansatz equations

Impose periodic boundary conditions in the horizontal direction. This means that the wave function must not change if the leftmost particle (L at x_1 or R at y_1) is moved to the corresponding position at the other (right) side of the system:

$$\begin{aligned} \psi(\text{L } x_1, \dots) &= \psi(\dots, \text{L } x_1 + L), \\ \psi(\text{R } y_1, \dots) &= \psi(\dots, \text{R } y_1 + L). \end{aligned}$$

The eigenfunction ψ given by (22) satisfies these conditions if the Bethe Ansatz equations (BAEs) hold:

$$u_i^L = (-)^{n_L-1} \prod_{j=1}^{n_R} S_{u_i v_j}, \quad (24)$$

$$v_j^L = (-)^{n_R-1} \prod_{i=1}^{n_L} S_{u_i v_j}^{-1}. \quad (25)$$

Note that although the description of an eigenfunction in terms of the u and v involves factors (17) and (18), the BAEs only contain factors (19).

Upon substitution of

$$u = \left(\frac{w_0^3 w_3 w_4}{w_1 w_2 w_5^3} \right)^{\frac{1}{2}} \xi \quad \text{and} \quad v = - \left(\frac{w_1^3 w_4 w_5}{w_0^3 w_2 w_3} \right)^{\frac{1}{2}} \eta^{-1} \quad (26)$$

the expression (19) for S_{uv} simplifies to

$$S_{uv} = \left(\frac{w_0 w_2 w_4}{w_1 w_3 w_5} \right)^{\frac{1}{2}} \frac{\eta - \xi}{1 + \xi \eta}.$$

The BAEs (24) and (25) can then be written

$$\left(\frac{w_0^3 w_3 w_4}{w_1 w_2 w_5^3} \right)^{\frac{1}{2}L} \left(\frac{w_1 w_3 w_5}{w_0 w_2 w_4} \right)^{\frac{1}{2}n_R} \xi_i^L = (-)^{n_L + n_R - 1} \prod_{j=1}^{n_R} \eta_j^{-1} \frac{\xi_i - \eta_j}{\xi_i + \eta_j^{-1}}, \quad (27)$$

$$\left(\frac{w_1^3 w_4 w_5}{w_0^3 w_2 w_3} \right)^{\frac{1}{2}L} \left(\frac{w_1 w_3 w_5}{w_0 w_2 w_4} \right)^{\frac{1}{2}n_L} \eta_j^L = (-)^{L + n_R - 1} \prod_{i=1}^{n_L} \xi_i^{-1} \frac{\eta_j - \xi_i}{\eta_j + \xi_i^{-1}}. \quad (28)$$

These equations can be considered the key result in the exact solution of the model. They determine the possible values for the ξ and the η . These in turn determine the eigenvalues and the eigenfunctions of the transfer matrix,

$$\Lambda = w_0^L \left(\frac{w_3 w_4 w_5}{w_0 w_1 w_2} \right)^{\frac{1}{4}n_L} \left(\frac{w_1 w_2 w_3}{w_0 w_4 w_5} \right)^{\frac{1}{4}n_R} \left(\prod_{i=1}^{n_L} \xi_i \prod_{j=1}^{n_R} (-\eta_j) \right)^{\frac{1}{2}}, \quad (29)$$

where we have reintroduced the factor w_0^L that was omitted as of Subsection 3.1.

As a check on the Bethe Ansatz we determined the eigenvalues of the transfer matrix for small system size by (brute force) numerical diagonalisation; the same eigenvalues were obtained by numerically solving the BAEs.

4 Thermodynamics

We are interested in the behaviour of the model as a function of the sub-lattice densities, that is, the canonical ensemble. In order to set up a transfer matrix we have passed to the grand canonical ensemble, which is controlled by sub-lattice weights (or chemical potentials) instead of sub-lattice densities. In this section it turns out that the transfer matrix leads to a semi-grand canonical ensemble. It is controlled partly by densities (essentially the two conserved quantities) and partly by chemical potentials. We describe the Legendre transformation from this ensemble back to the canonical ensemble. We also look into the symmetries between the sub-lattices and how they appear in the semi-grand canonical ensemble.

4.1 Legendre transformation

In passing to the grand canonical ensemble each trimer on a sub-lattice i was given a weight $w_i = \exp(\mu_i)$. Certain combinations of these weights occur in the BAEs (27) and (28) and in the expression (29) of the transfer matrix eigenvalue in terms of the BA roots. It is convenient to

assign names to the corresponding combinations of the chemical potentials $\mu_i = \log w_i$,

$$\begin{aligned}\phi_L &= \frac{1}{2}[(3\mu_0 - \mu_1 - \mu_2 + \mu_3 + \mu_4 - 3\mu_5) + \rho_R(-\mu_0 + \mu_1 - \mu_2 + \mu_3 - \mu_4 + \mu_5)], \\ \phi_R &= \frac{1}{2}[(3\mu_0 - 3\mu_1 + \mu_2 + \mu_3 - \mu_4 - \mu_5) + \rho_L(-\mu_0 + \mu_1 - \mu_2 + \mu_3 - \mu_4 + \mu_5)], \\ \mu_L &= \frac{1}{4}(-\mu_0 - \mu_1 - \mu_2 + \mu_3 + \mu_4 + \mu_5), \\ \mu_R &= \frac{1}{4}(-\mu_0 + \mu_1 + \mu_2 + \mu_3 - \mu_4 - \mu_5),\end{aligned}$$

where

$$\rho_L = \frac{n_L}{L} \quad \text{and} \quad \rho_R = \frac{n_R}{L}$$

denote the densities of the particles L and R. With these definitions the BAEs (27) and (28) can be written

$$(e^{\phi_L \xi_i})^L = (-)^{n_L+n_R-1} \prod_{j=1}^{n_R} \eta_j^{-1} \frac{\xi_i - \eta_j}{\xi_i + \eta_j^{-1}}, \quad (30)$$

$$(e^{\phi_R \eta_j})^L = (-)^{L+n_R-1} \prod_{i=1}^{n_L} \xi_i^{-1} \frac{\eta_j - \xi_i}{\eta_j + \xi_i^{-1}}, \quad (31)$$

while the eigenvalue expression (29) becomes

$$\Lambda = \exp(L\mu_0 + n_L\mu_L + n_R\mu_R) \left(\prod_{i=1}^{n_L} \xi_i \prod_{j=1}^{n_R} (-\eta_j) \right)^{\frac{1}{2}}. \quad (32)$$

Taking the logarithm, dividing by L , and letting L to infinity gives the free energy per trimer in the thermodynamic limit:

$$\Omega(\rho_L, \rho_R; \mu_0, \mu_1, \dots, \mu_5) = \Phi(\rho_L, \rho_R; \phi_L, \phi_R) - \rho_L\mu_L - \rho_R\mu_R - \mu_0,$$

where

$$\Phi(\rho_L, \rho_R; \phi_L, \phi_R) = - \lim_{L \rightarrow \infty} \frac{1}{L} \log \left(\prod_{i=1}^{n_L} \xi_i \prod_{j=1}^{n_R} (-\eta_j) \right)^{\frac{1}{2}}. \quad (33)$$

It is the free energy in a semi-grand canonical ensemble where the numbers of trimers on the different sub-lattices may vary but are subject to the constraints imposed by fixing the particle densities

$$\rho_L = 1 - \rho_0 - \rho_1 + \rho_3 + \rho_4, \quad (34)$$

$$\rho_R = 1 - \rho_0 + \rho_2 + \rho_3 - \rho_5. \quad (35)$$

In order to do the Legendre transform to the canonical ensemble the derivatives of Ω with respect to $\mu_0, \mu_1, \dots, \mu_5$ have to be taken. This gives the ensemble average densities

$$\rho_0 = \left(-\frac{3}{2} + \frac{1}{2}\rho_R\right) \frac{\partial\Phi}{\partial\phi_L} + \left(-\frac{3}{2} + \frac{1}{2}\rho_L\right) \frac{\partial\Phi}{\partial\phi_R} - \frac{1}{4}\rho_L - \frac{1}{4}\rho_R + 1. \quad (36)$$

$$\rho_1 = \left(+\frac{1}{2} - \frac{1}{2}\rho_R\right) \frac{\partial\Phi}{\partial\phi_L} + \left(+\frac{3}{2} - \frac{1}{2}\rho_L\right) \frac{\partial\Phi}{\partial\phi_R} - \frac{1}{4}\rho_L + \frac{1}{4}\rho_R, \quad (37)$$

$$\rho_2 = \left(+\frac{1}{2} + \frac{1}{2}\rho_R\right) \frac{\partial\Phi}{\partial\phi_L} + \left(-\frac{1}{2} + \frac{1}{2}\rho_L\right) \frac{\partial\Phi}{\partial\phi_R} - \frac{1}{4}\rho_L + \frac{1}{4}\rho_R, \quad (38)$$

$$\rho_3 = \left(-\frac{1}{2} - \frac{1}{2}\rho_R\right) \frac{\partial\Phi}{\partial\phi_L} + \left(-\frac{1}{2} - \frac{1}{2}\rho_L\right) \frac{\partial\Phi}{\partial\phi_R} + \frac{1}{4}\rho_L + \frac{1}{4}\rho_R, \quad (39)$$

$$\rho_4 = \left(-\frac{1}{2} + \frac{1}{2}\rho_R\right) \frac{\partial\Phi}{\partial\phi_L} + \left(+\frac{1}{2} + \frac{1}{2}\rho_L\right) \frac{\partial\Phi}{\partial\phi_R} + \frac{1}{4}\rho_L - \frac{1}{4}\rho_R, \quad (40)$$

$$\rho_5 = \left(+\frac{3}{2} - \frac{1}{2}\rho_R\right) \frac{\partial\Phi}{\partial\phi_L} + \left(+\frac{1}{2} - \frac{1}{2}\rho_L\right) \frac{\partial\Phi}{\partial\phi_R} + \frac{1}{4}\rho_L - \frac{1}{4}\rho_R. \quad (41)$$

In Subsection 2.1 it was seen that because the sub-lattice densities satisfy two constraints, four of them are independent. Equations (36)–(41) express the sub-lattice densities in terms of only four quantities, namely $\rho_L, \rho_R, \frac{\partial\Phi}{\partial\phi_L}$ and $\frac{\partial\Phi}{\partial\phi_R}$. Therefore these four quantities must be independent, and the sub-lattice densities given by (36)–(41) must satisfy the two constraints, (1) and (2). This can also be verified by direct computation. The entropy per trimer is

$$S(\rho_0, \rho_1, \dots, \rho_5) = -\Omega + \sum_{\ell=0}^5 \rho_\ell \mu_\ell = -\Phi + \frac{\partial\Phi}{\partial\phi_L} \phi_L + \frac{\partial\Phi}{\partial\phi_R} \phi_R. \quad (42)$$

It is remarkable that the chemical potentials μ_0, μ_L and μ_R that occur in the expression (32) for the eigenvalue have disappeared in the Legendre transformation. As a consequence Φ and hence the densities $\rho_0, \rho_1, \dots, \rho_5$ and the entropy S are now functions of four parameters: the particle densities ρ_L and ρ_R and the potential-like quantities ϕ_L and ϕ_R . These are just the parameters that govern the BAEs (30) and (31). This agrees with the fact that the canonical ensemble also has four parameters.

4.2 Symmetries of the parameter space

For the reference state of the BA sub-lattice 0 was chosen. Since the model is invariant under horizontal translations over a single lattice edge sub-lattice 2 (or 4) could have been chosen instead. The original situation can be regained by renumbering the sub-lattices $i \rightarrow i - 2 \pmod{6}$. The sub-lattice densities ρ'_i in the new numbering are related to the densities ρ_i in the old numbering by

$$\rho'_0 = \rho_2, \quad \rho'_1 = \rho_3, \quad \text{etc.} \quad (43)$$

and analogously for the chemical potentials μ_i . From this one computes

$$\rho'_L = 2 - \rho_R, \quad \rho'_R = 1 + \rho_L - \rho_R, \quad \phi'_L = -\phi_L + \phi_R, \quad \phi'_R = -\phi_L.$$

Similarly the model is invariant under reflection in a horizontal line. The corresponding sub-lattice renumbering is $i \rightarrow i + 3 \pmod{6}$. This gives:

$$\rho'_L = 2 - \rho_L, \quad \rho'_R = 2 - \rho_R, \quad \phi'_L = \phi_L, \quad \phi'_R = \phi_R.$$

The model is also invariant under reflection in a vertical line. For the line passing through sub-lattices 0 and 3 the renumbering is $i \rightarrow -i \pmod{6}$. Obviously this is nothing but interchanging left and right, so

$$\rho'_L = \rho_R, \quad \rho'_R = \rho_L, \quad \phi'_L = \phi_R, \quad \phi'_R = \phi_L.$$

Together these three transformations generate a group of order twelve. In Subsection 6.3 we shall find four “families” of points in the parameter space where the entropy of the model can be computed exactly. These four families turn out to be related by symmetries from this group. Note that under this symmetry group the free energy Ω and the entropy S are invariant, so Φ transforms in a certain way. For example, for the translation (43) the transformation is

$$\Phi(2 - \rho_R, 1 + \rho_L - \rho_R; -\phi_L + \phi_R, -\phi_L) = \Phi(\rho_L, \rho_R; \phi_L, \phi_R) - \frac{1}{2}\phi_L.$$

Finally the model is invariant under some rotations. As an example, consider the rotation over $2\pi/3$ about an up triangle of the lattice. The sub-lattice renumbering is: $1 \rightarrow 3 \rightarrow 5$. This does not give a simple transformation of ρ_L, ρ_R, ϕ_L and ϕ_R . This can be explained as follows. In the definition of these four parameters the direction in which the transfer matrix acts plays a special role. Rotations do not preserve this direction, in contrast to the translation and the two reflections described above. The symmetry group generated by all these operations is of order 36.

5 Integral equations

In Section 3 two sets of BAEs were derived. These equations can be solved numerically, for system size L up to a few hundred, say. This can be done essentially in the full parameter space. (The regions where numerical complications arise can be mapped to regions without such difficulties by means of symmetries from Subsection 4.2.) We however want to get analytic expressions for the physical quantities of the model in thermodynamic limit. In the present section the BAEs in the thermodynamic limit are turned into two integral equations for two complex functions. These functions are multivalued, and their monodromy properties are obtained from the integral equations. The functions are then determined from their monodromy and analyticity properties. In the next section these functions will be used to compute physical quantities of the model.

5.1 Derivation

We shall now in the usual fashion derive integral equations from the BAEs (30) and (31). The logarithmic version of these BAEs is

$$LF_L(\xi_i) \equiv (n_L + n_R - 1)\pi i \pmod{2\pi i}, \quad (44)$$

$$LF_R(\eta_j) \equiv (L + n_R - 1)\pi i \pmod{2\pi i}, \quad (45)$$

where

$$F_L(z) = \log z - \frac{1}{L} \sum_{j=1}^{n_R} [\log(z - \eta_j) - \log(z + \eta_j^{-1})] + \phi_L + \frac{1}{L} \sum_{j=1}^{n_R} \log \eta_j, \quad (46)$$

$$F_R(z) = \log z - \frac{1}{L} \sum_{i=1}^{n_L} [\log(z - \xi_i) - \log(z + \xi_i^{-1})] + \phi_R + \frac{1}{L} \sum_{i=1}^{n_L} \log \xi_i. \quad (47)$$

The derivatives of these functions are

$$f_L(z) = \frac{1}{z} - \frac{1}{L} \sum_{j=1}^{n_R} \left(\frac{1}{z - \eta_j} - \frac{1}{z + \eta_j^{-1}} \right), \quad (48)$$

$$f_R(z) = \frac{1}{z} - \frac{1}{L} \sum_{i=1}^{n_L} \left(\frac{1}{z - \xi_i} - \frac{1}{z + \xi_i^{-1}} \right). \quad (49)$$

For the understanding of the structure of the solutions to the BAEs we rely on numeric computations for finite system size. For many values of the parameters ρ_L, ρ_R, ϕ_L and ϕ_R the BA roots for the largest eigenvalue show the following features. The roots ξ_i and η_j lie on smooth curves

in the complex plane. When the system size becomes large these curves tend to well-defined limit shapes. These limit curves will be called Ξ and H . The sets $\{\xi_i\}$ and $\{\eta_j\}$ (and hence also the curves Ξ and H) are invariant under complex conjugation; this implies that

$$f_L(z^*) = f_L(z)^* \quad \text{and} \quad f_R(z^*) = f_R(z)^*. \quad (50)$$

The curve Ξ crosses the positive real axis, whereas H crosses the negative real axis. Note that by (44) the roots ξ_i are solutions of

$$L F_L(\xi) \equiv (n_L + n_R - 1)\pi i \pmod{2\pi i}. \quad (51)$$

This equation defines discrete points on the curve $\text{Re } F_L(\xi) = 0$. The roots ξ_i occupy a succession of these points, without holes:

$$L [F_L(\xi_{i+1}) - F_L(\xi_i)] = 2\pi i. \quad (52)$$

By holes we mean solutions of (51) lying between ξ_1 and ξ_{n_L} on the curve $\text{Re } F_L(\xi) = 0$ that are not contained in the set $\{\xi_i\}$. Similary for $\{\eta_j\}$:

$$L [F_R(\eta_{j+1}) - F_R(\eta_j)] = 2\pi i. \quad (53)$$

Let b_L and b_R denote the end points in the upper half plane of Ξ and H . When the system becomes large ξ_1 and ξ_{n_L} tend to b_L^* and b_L , respectively, while η_1 and η_{n_R} tend to b_R and b_R^* , respectively. Figure 7 shows the distribution of the roots for the largest eigenvalue in a given sector n_L, n_R .

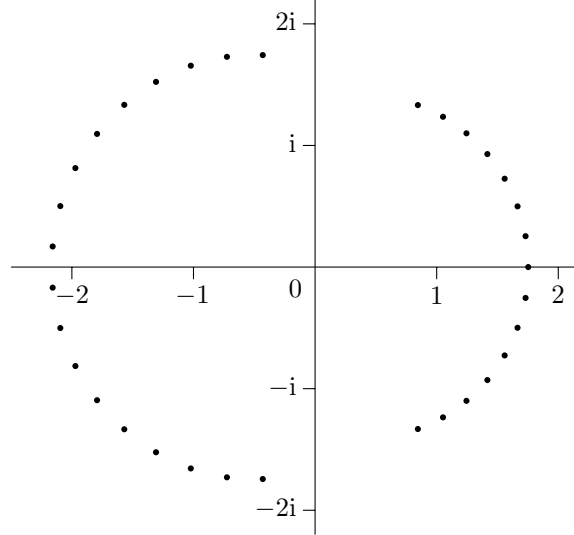


Figure 7: Distribution of the BAE roots for the largest eigenvalue. The ξ are on the right, the η on the left. The parameters have the values $\phi_L = -0.46$, $\phi_R = -0.653$, $n_L = 15$, $n_R = 18$ and $L = 30$.

We assume that the condition that there are no holes in the sets of roots $\{\xi_i\}$ and $\{\eta_j\}$ also holds in the thermodynamic limit. There (52) and (53) can be written

$$L f_L(\xi_i)(\xi_{i+1} - \xi_i) = 2\pi i, \quad (54)$$

$$L f_R(\eta_j)(\eta_{j+1} - \eta_j) = 2\pi i, \quad (55)$$

so that the sums in (48) and (49) can be turned into integrals

$$f_L(z) = \frac{1}{z} + \frac{1}{2\pi i} \int_H \left(\frac{1}{\eta - z} + \frac{1}{\eta^{-1} + z} \right) f_R(\eta) d\eta, \quad (56)$$

$$f_R(z) = \frac{1}{z} + \frac{1}{2\pi i} \int_\Xi \left(\frac{1}{\xi - z} + \frac{1}{\xi^{-1} + z} \right) f_L(\xi) d\xi. \quad (57)$$

From these equations it is seen that $f_L(z)$ has branch cuts H and $-H^{-1}$ and that $f_R(z)$ has branch cuts Ξ and $-\Xi^{-1}$. From the same equations it is easily computed that $zf_L(z)$ and $zf_R(z)$ are invariant under $z \mapsto -z^{-1}$. Therefore we substitute

$$z - z^{-1} = \hat{z}, \quad (58)$$

and define

$$zf_L(z) = g_L(\hat{z}) \quad \text{and} \quad zf_R(z) = g_R(\hat{z}). \quad (59)$$

The two branch cuts H and $-H^{-1}$ of $f_L(z)$ then collapse to a single branch cut \hat{H} of $g_L(\hat{z})$, and similarly for $f_R(z)$. The equations (56) and (57) become

$$g_L(\hat{z}) = 1 + \frac{1}{2\pi i} \int_{\hat{H}} \frac{1}{\hat{\eta} - \hat{z}} g_R(\hat{\eta}) d\hat{\eta}, \quad (60)$$

$$g_R(\hat{z}) = 1 + \frac{1}{2\pi i} \int_{\hat{\Xi}} \frac{1}{\hat{\xi} - \hat{z}} g_L(\hat{\xi}) d\hat{\xi}. \quad (61)$$

The functions $f_L(z)$ and $f_R(z)$ and hence also $g_L(\hat{z})$ and $g_R(\hat{z})$ contain all information about the BA roots ξ_i and η_j that is needed to compute the densities ρ_L and ρ_R , the phases ϕ_L and ϕ_R , and the semi-grand canonical free energy Φ .

The integral equations (60) and (61) are very similar to the equations obtained by Kalugin [16] for the square-triangle random tiling model. He tackles his equations by exploiting the monodromy properties of the functions. We shall use the same method for our integral equations, closely following Kalugin's argument.

5.2 Monodromy properties

The first step in solving the integral equations (60) and (61) (but only for a special case to be defined below) is to establish the monodromy properties of the functions $g_L(\hat{z})$ and $g_R(\hat{z})$. From (60) it is seen that the contour \hat{H} is a branch cut of the function $g_L(\hat{z})$. Consider this function on a path $\Gamma_{\hat{H}}$ that crosses the contour \hat{H} in some point \hat{z}_0 , as in Figure 8(a). The jump of the function g_L over the contour is

$$g_L(\hat{z}_0)_{\text{after}} - g_L(\hat{z}_0)_{\text{before}} = \frac{1}{2\pi i} \oint_{|\hat{\eta} - \hat{z}_0| = \varepsilon} \frac{1}{\hat{\eta} - \hat{z}_0} g_R(\hat{\eta}) d\hat{\eta} = g_R(\hat{z}_0).$$

Hence the analytic continuation of $g_L(\hat{z})$ along the path $\Gamma_{\hat{H}}$ through the contour \hat{H} is $g_L(\hat{z}) - g_R(\hat{z})$. From (61) the contour \hat{H} is not a branch cut of the function $g_R(\hat{z})$, so the analytic continuation of $g_R(\hat{z})$ along $\Gamma_{\hat{H}}$ is just $g_R(\hat{z})$. Therefore the effect of analytic continuation along $\Gamma_{\hat{H}}$ on a linear combination $a_L g_L(\hat{z}) + a_R g_R(\hat{z})$ is given by

$$\Gamma_{\hat{H}} : \begin{pmatrix} a_L \\ a_R \end{pmatrix} \mapsto \begin{pmatrix} 1 & 0 \\ -1 & 1 \end{pmatrix} \begin{pmatrix} a_L \\ a_R \end{pmatrix}.$$

It can be derived analogously that the monodromy operator for the path $\Gamma_{\hat{\Xi}}$ in Figure 8(a) is given by

$$\Gamma_{\hat{\Xi}} : \begin{pmatrix} a_L \\ a_R \end{pmatrix} \mapsto \begin{pmatrix} 1 & 1 \\ 0 & 1 \end{pmatrix} \begin{pmatrix} a_L \\ a_R \end{pmatrix}.$$

The operators $\Gamma_{\hat{H}}$ and $\Gamma_{\hat{\Xi}}$ generate the full group $\text{SL}(2, \mathbf{Z})$. Now consider the special case that the end points \hat{b}_L and \hat{b}_L^* of $\hat{\Xi}$ coincide with the end points \hat{b}_R and \hat{b}_R^* of \hat{H} , and that the contours do not meet in other points. Then the paths $\Gamma_{\hat{H}}$ and $\Gamma_{\hat{\Xi}}$ are no longer defined, but their composite

$\Gamma_{\hat{H}}\Gamma_{\hat{\Xi}}$ is, see Figure 8(b). Since this operator is of order six $g_L(\hat{z})$ and $g_R(\hat{z})$ are single-valued functions of the variable

$$t = \left(\frac{\hat{z} - \hat{b}}{\hat{z} - \hat{b}^*} \right)^{1/6}, \quad (62)$$

where $\hat{b} = \hat{b}_L = \hat{b}_R$ and $\hat{b}^* = \hat{b}_L^* = \hat{b}_R^*$ are the common end points of the contours. The inverse transformation is

$$\hat{z} = \frac{\hat{b}^* t^6 - \hat{b}}{t^6 - 1}.$$

Since $(\Gamma_{\hat{H}}\Gamma_{\hat{\Xi}})g_R(\hat{z}) = g_L(\hat{z})$, the functions $g_L(\hat{z})$ and $g_R(\hat{z})$ are different branches of a single function $g(\hat{z})$.

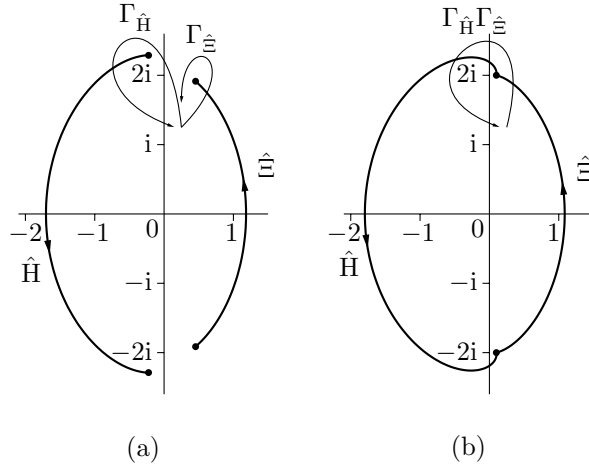


Figure 8: The contours $\hat{\Xi}$ and \hat{H} . ($\phi_L = -0.46$, $\phi_R = -0.653$ and (a) $\rho_L = 0.5$, $\rho_R = 0.6$, (b) $\rho_L = 0.76$, $\rho_R = 0.93$.)

In the remainder of this paper we shall, unless stated otherwise, consider the case that the end points of the contours $\hat{\Xi}$ and \hat{H} coincide, and that these are the only common points of these contours.

5.3 Analyticity properties

It follows from (60) that $g_L(\hat{z})$ is analytic everywhere except on the branch cut \hat{H} . Similarly $g_R(\hat{z})$ is analytic everywhere except on $\hat{\Xi}$. In particular it is analytic on the contour \hat{H} , except perhaps at the end points, as these lie also on $\hat{\Xi}$. It then follows from (60) that $g_L(\hat{z})$ remains finite if \hat{z} approaches a point (not an end point) on its branch cut \hat{H} . An analogous statement holds for $g_R(\hat{z})$. To summarise, $g_L(\hat{z})$ and $g_R(\hat{z})$ are finite everywhere except perhaps at \hat{b} and \hat{b}^* .

It was derived above that they are branches of one function $g(\hat{z})$, which in turn is a single-valued function of t . Fix this function $h(t)$ by choosing that at $t = e^{\pi i/3}$ it corresponds to $g_L(\hat{z})$ (at $\hat{z} = \infty$). Figure 9 shows where in the t -plane all the branches of $g(\hat{z}) = h(t)$ are situated. Note that the branch at $t = e^{-\pi i/3}$ is $g_R(\hat{z})$ (at $\hat{z} = \infty$).

Since $g(\hat{z})$ is finite everywhere except perhaps at $\hat{z} = \hat{b}$ and $\hat{z} = \hat{b}^*$, $h(t)$ is analytic everywhere except perhaps at $t = 0$ and $t = \infty$. Because $h(t)$ is single-valued it can only have power singularities (with integer exponent). Now

$$\rho_L = \frac{1}{2\pi} \int_{\hat{\Xi}} f_L(z) dz = \frac{1}{2\pi} \int_{\hat{\Xi}} g_L(\hat{z}) \frac{dz}{d\hat{z}} d\hat{z} = \frac{1}{2\pi} \int_{\infty}^0 h(t) \frac{dz}{d\hat{z}} \frac{d\hat{z}}{dt} dt, \quad (63)$$

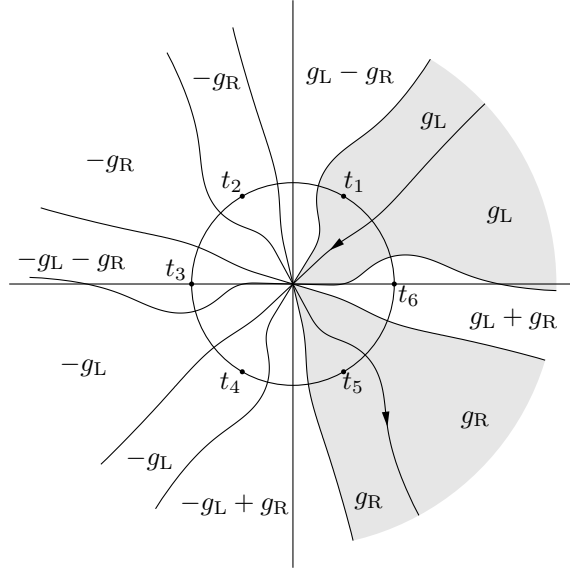


Figure 9: The complex t -plane. The contours corresponding to $\hat{\Xi}$ and \hat{H} divide the plane into sectors that correspond to different branches of the function $g(\hat{z})$. The shaded regions correspond to $g_L(\hat{z})$ and $g_R(\hat{z})$. (The interest of this picture lies in its qualitative features, but it was actually computed from a numerical solution of the BAEs. The parameters are $\phi_L = -0.46$, $\phi_R = -0.653$, $n_L = 152$, $n_R = 186$, and $L = 200$. These values correspond to $\hat{b} = 2ie^{-0.05i}$.)

where the last integral is over some contour running from ∞ to 0 , is finite. Since $\frac{d\hat{z}}{dt}$ remains finite and non-zero for t near 0 or ∞ , and

$$\frac{d\hat{z}}{dt} = \frac{6(\hat{b} - \hat{b}^*)t^5}{(t^6 - 1)^2} \sim \begin{cases} t^5 & \text{if } t \rightarrow 0, \\ t^{-7} & \text{if } t \rightarrow \infty, \end{cases}$$

it follows that $h(t)$ has at worst singularities t^{-5} at $t = 0$ and t^5 at $t = \infty$. Hence, the 1-form

$$g(\hat{z}) d\hat{z} = h(t) \frac{d\hat{z}}{dt} dt$$

is nonsingular at $t = 0$ and $t = \infty$.

5.4 Calculation of $g(\hat{z})$

In the previous subsection it was shown that the 1-form (5.3) is nonsingular at $t = 0$ and $t = \infty$. The only singularities it can have are second order poles at the zeros t_1, t_2, \dots, t_6 of $t^6 - 1$. (These are the points in the t -plane corresponding to $\hat{z} = \infty$.) Therefore it can be written as

$$g(\hat{z}) d\hat{z} = h(t) \frac{d\hat{z}}{dt} dt = \sum_{k=1}^6 \left\{ \frac{r_k}{t - t_k} + \frac{s_k}{(t - t_k)^2} \right\} dt.$$

The coefficients r_k and s_k are given by

$$r_k = \text{Res}_{t=t_k} h(t) \frac{d\hat{z}}{dt} dt = \text{Res}_{\hat{z}=\infty} g(\hat{z}) d\hat{z}.$$

and

$$s_k = \text{Res}_{t=t_k} (t - t_k) h(t) \frac{d\hat{z}}{dt} dt = \left[(t - t_k) \hat{z} \right]_{t=t_k} \text{Res}_{\hat{z}=\infty} \hat{z}^{-1} g(\hat{z}) d\hat{z},$$

where the appropriate branch of $g(\hat{z})$ is to be taken.

The residues $\text{Res}_{\hat{z}=\infty} g(\hat{z})d\hat{z}$ and $\text{Res}_{\hat{z}=\infty} \hat{z}^{-1}g(\hat{z})d\hat{z}$ still have to be computed. From (60) and (61) one has

$$\begin{aligned}\text{Res}_{\hat{z}=\infty} g_L(\hat{z})d\hat{z} &= -\frac{1}{2\pi i} \int_{\hat{H}} g_R(\hat{\eta}) d\hat{\eta} =: R_L, \\ \text{Res}_{\hat{z}=\infty} g_R(\hat{z})d\hat{z} &= -\frac{1}{2\pi i} \int_{\hat{\Xi}} g_L(\hat{\xi}) d\hat{\xi} =: R_R\end{aligned}$$

and

$$\begin{aligned}\text{Res}_{\hat{z}=\infty} \hat{z}^{-1}g_L(\hat{z})d\hat{z} &= -1, \\ \text{Res}_{\hat{z}=\infty} \hat{z}^{-1}g_R(\hat{z})d\hat{z} &= -1.\end{aligned}$$

The residues for the other branches of $g(\hat{z})$ follow by application of the monodromy operators. They are listed in Table 2. It follows from (50) that the integrals R_L and R_R are real.

Table 2: The poles and residues of $g(\hat{z})d\hat{z}$.

k	t_k	g	$\text{Res}_{\hat{z}=\infty} g(\hat{z})d\hat{z}$	$\text{Res}_{\hat{z}=\infty} \hat{z}^{-1}g(\hat{z})d\hat{z}$
1	$e^{\pi i/3}$	g_L	R_L	-1
2	$-e^{-\pi i/3}$	$-g_R$	$-R_R$	1
3	-1	$-g_L - g_R$	$-R_L - R_R$	2
4	$-e^{\pi i/3}$	$-g_L$	$-R_L$	1
5	$e^{-\pi i/3}$	g_R	R_R	-1
6	1	$g_L + g_R$	$R_L + R_R$	-2

Combining these results gives after some algebra that

$$\begin{aligned}g(\hat{z}) &= \sum_{k=1}^6 \left\{ \frac{r_k}{t - t_k} + \frac{s_k}{(t - t_k)^2} \right\} \left(\frac{d\hat{z}}{dt} \right)^{-1} \\ &= (1 - 2C)t + (1 - 2C^*)t^{-1} + C(t + t^{-5}) + C^*(t^{-1} + t^5)\end{aligned}\quad (64)$$

with

$$C = \frac{1}{6} + \frac{1}{2\sqrt{3}\text{Im } \hat{b}} \left[e^{\pi i/3} R_L - e^{-\pi i/3} R_R \right].$$

We shall now argue in the generic case, $\hat{b} \neq 2i$, that $C = 0$. From (54) and (55) the curves Ξ and H are described by $\text{Re}[f_L(z) dz] = 0$ and $\text{Re}[f_R(z) dz] = 0$, respectively, so the corresponding curves in the t -plane are both solutions of

$$\text{Re} \left[\frac{g(\hat{z})}{z} \frac{dz}{d\hat{z}} \frac{d\hat{z}}{dt} dt \right] = 0. \quad (65)$$

Note that z and $\frac{dz}{d\hat{z}}$ are not single-valued functions of t , but the two branches of

$$\frac{1}{z} \frac{dz}{d\hat{z}} = \frac{1}{z + z^{-1}} = \frac{1}{\sqrt{\hat{z}^2 + 4}}$$

differ only by a sign, which does not influence (65). The two different solutions of (65) corresponding to Ξ and H , respectively, meet at $t = 0$ (and at $t = \infty$), so at these points the differential equation admits multiple solutions. When $t \rightarrow 0$

$$\frac{g(\hat{z})}{z} \frac{dz}{d\hat{z}} \frac{d\hat{z}}{dt} dt = 6 \frac{\hat{b} - \hat{b}^*}{\hat{b} + \hat{b}^{-1}} \left[C + (1 - C)^* t^4 + O(t^6) \right] dt,$$

so this implies that $C = 0$.

We shall now argue in the special case $\hat{b} = 2i$ that $C = 0$. When $t \rightarrow 0$

$$f(z) dz = \frac{g(\hat{z})}{z} \frac{dz}{d\hat{z}} \frac{d\hat{z}}{dt} dt = 6 [Ct^{-3} + (1-C)^*t + O(t^3)] dt$$

(and similarly when $t \rightarrow \infty$). The finiteness of the integral (63) (or its analogue for ρ_R) implies that $C = 0$.

Now (64) becomes

$$g(\hat{z}) = t + t^{-1}. \quad (66)$$

The functions $g_L(\hat{z})$ and $g_R(\hat{z})$ are obtained by taking the appropriate branches $t_L(\hat{z})$ and $t_R(\hat{z})$ of $t(\hat{z})$. The branch $t_L(\hat{z})$ is determined by $t_L(\infty) = e^{\pi i/3}$ and the fact that it has \hat{H} as its only branch cut. Similarly $t_R(\hat{z})$ is determined by $t_R(\infty) = e^{-\pi i/3}$ and the fact that it has $\hat{\Xi}$ as its only branch cut.

6 Calculation of physical quantities

In Section 4 the relation was established between the canonical ensemble we are interested in and the semi-grand canonical ensemble that arises in the BA from Section 3. In Section 5 BA information was encoded in two complex functions satisfying a set of integral equations. These functions were then solved from those equations. In the present section the physical quantities occurring in Section 4 are extracted from the complex functions determined in Section 5.

6.1 Calculation of ρ_L , ρ_R , ϕ_L , ϕ_R , and Φ

From (59) and (66) $f_L(z)$ and $f_R(z)$ are both given by

$$f(z) = \frac{t + t^{-1}}{z}, \quad (67)$$

with different branches of t . It was claimed in Subsection 5.1 that the BA parameters ρ_L , ρ_R , ϕ_L and ϕ_R and the semi-grand canonical free energy Φ can be computed from the functions $f_L(z)$ and $f_R(z)$. They depend on the point \hat{b} . The particle density ρ_L was already computed in (63):

$$\rho_L = \frac{1}{2\pi i} \int_{\Xi} f_L(z) dz. \quad (68)$$

Because $f_L(z)$ is analytic this integral does not depend on the precise shape of Ξ , but on its homology only.

Next ϕ_L is calculated. Since $f_L(z)$ is known the function $F_L(z)$ is determined up to an integration constant. The real part of this integration constant is fixed by $\text{Re } F_L(b_L) = 0$, see (44). From (46) one has

$$\text{Re} [F_L(z) + F_L(-z^{-1})] = 2\phi_L.$$

It is now easy to compute that

$$\phi_L = \frac{1}{2} \text{Re} \int_{b_L}^{-b_L^{-1}} f_L(z) dz. \quad (69)$$

From (33) the free energy Φ equals $-(\Sigma_L + \Sigma_R)$ with

$$\begin{aligned} \Sigma_L &= \lim_{L \rightarrow \infty} \frac{1}{2} \frac{1}{L} \sum_{j=1}^{n_R} \log |\eta_j|, \\ \Sigma_R &= \lim_{L \rightarrow \infty} \frac{1}{2} \frac{1}{L} \sum_{i=1}^{n_L} \log |\xi_i|. \end{aligned}$$

Using (46) one calculates

$$\operatorname{Re}[F_L(z) - \log z] \Big|_0^\infty = 2 \frac{1}{L} \sum_{j=1}^{m_R} \log |\eta_j|,$$

so

$$\Sigma_L = \frac{1}{4} \operatorname{Re} \int_0^\infty \left(f_L(z) - \frac{1}{z} \right) dz. \quad (70)$$

In (69) and (70) the integral again only depends on the homology of the integration path, not on its precise shape. The real part of the integral even does not depend at all on the path chosen between the integration end points, but the imaginary part does. This is because the indefinite integral (46) is a sum of logarithms with real prefactors, and distinct branches of a logarithm differ by a multiple of $2\pi i$, which is purely imaginary.

Replacing all subscripts L in (68), (69) and (70) with R yields expressions of ρ_R , ϕ_R , and Σ_R as integrals of functions involving $f_R(z)$. These integrals for ρ_L , ρ_R , ϕ_L , ϕ_R , Σ_L and Σ_R are of the form $\int y dz$, where the points (y, z) lie on an algebraic curve of genus 5. Therefore the indefinite integrals cannot be expressed in terms of “standard” functions. This does not prove that the definite integrals we need cannot be expressed in terms of standard functions, but it seems unlikely that it can be done. Of course they can be evaluated numerically.

6.2 Calculation of $\frac{\partial \Phi}{\partial \phi_L}$ and $\frac{\partial \Phi}{\partial \phi_R}$

The Legendre transformation in Subsection 4.1 involves the derivatives $\frac{\partial \Phi}{\partial \phi_L}$ and $\frac{\partial \Phi}{\partial \phi_R}$. Unfortunately we have not been able to compute Φ as a function of ρ_L , ρ_R , ϕ_L , and ϕ_R for all values of these arguments. Instead we have in Subsection 6.1 computed these parameters and the free energy in the case that the curves Ξ and \hat{H} close, as a function of their common end point $\hat{b} = \hat{b}_L = \hat{b}_R$. In order to still obtain the derivatives $\frac{\partial \Phi}{\partial \phi_L}$ and $\frac{\partial \Phi}{\partial \phi_R}$ we resort to a perturbation analysis. The details can be found in Appendix A; here we only give some results. An infinitesimally small complex parameter C describes how far the curves open up. The thermodynamic parameters ρ_L , ρ_R , ϕ_L , ϕ_R and the free energy Φ then are functions of \hat{b} and C . If all their first-order partial derivatives are known, $\frac{\partial \Phi}{\partial \phi_L}$ and $\frac{\partial \Phi}{\partial \phi_R}$ can be found by applying the standard coordinate transformation formula to the transformation between coordinates $\operatorname{Re} \hat{b}$, $\operatorname{Im} \hat{b}$, $\operatorname{Re} C$ and $\operatorname{Im} C$ on the one hand and ρ_L , ρ_R , ϕ_L and ϕ_R on the other hand. The derivatives with respect to $\operatorname{Re} \hat{b}$ and $\operatorname{Im} \hat{b}$ can be obtained immediately from the integral expressions in Subsection 6.1. For the derivatives with respect to $\operatorname{Re} C$ and $\operatorname{Im} C$ the perturbation analysis is needed. It tells that to leading order in C the parameters ρ_L , ρ_R , ϕ_L , ϕ_R and the free energy $\Phi = -(\Sigma_L + \Sigma_R)$ are again given by the integrals (68), (69), (70) and their analogues involving $f_R(z)$, where $f(z)$ is now given by

$$f(z) = \frac{t + t^{-1} + C(t^{-5} - t) + C^*(t^5 - t^{-1})}{z}. \quad (71)$$

This yields integral expressions for their derivatives with respect to $\operatorname{Re} C$ and $\operatorname{Im} C$.

The expressions thus obtained for the partial derivatives of ρ_L , ρ_R , ϕ_L , ϕ_R and Φ with respect to $\operatorname{Re} \hat{b}$, $\operatorname{Im} \hat{b}$, $\operatorname{Re} C$ and $\operatorname{Im} C$ were evaluated numerically for some chosen value of \hat{b} , and from this $\frac{\partial \Phi}{\partial \phi_L}$ and $\frac{\partial \Phi}{\partial \phi_R}$ were calculated. These derivatives were also computed from numerical solutions of the BAEs for large system size L by numerical differentiation. The results from the two methods agree, which supports the perturbation analysis of Appendix A.

6.3 Configuration of Ξ and H

In the previous two sections several physical quantities have been expressed as integrals of functions involving $f_L(z)$ and $f_R(z)$. These integrals depend on the parameter \hat{b} and on the topology of the curves Ξ and H , but not on their precise shape. If $\hat{b} \neq 2i$ there are two distinct points in the z -plane

corresponding to \hat{b} , say b_1 and b_2 . The end points of Ξ could be b_1 and b_1^* or b_2 and b_2^* , and the same holds for H . Therefore one can expect at least four different configurations for one and the same value of \hat{b} . In order to determine what these four configurations actually are, we first guessed what they might look like. Then we chose some particular value of \hat{b} (close to $2i$) and for each of the four expected cases computed the value of the particle densities ρ_L and ρ_R and the phases ϕ_L and ϕ_R . The BAEs were solved numerically for these parameter values, for large system size L . The resulting curves followed by the ξ and the η display indeed the presupposed configurations. These curves are shown in Figure 10. Note that without first guessing the configurations we would have had no way to find the values of the parameters ρ_L , ρ_R , ϕ_L and ϕ_R , so there would have been no BAEs to solve numerically.

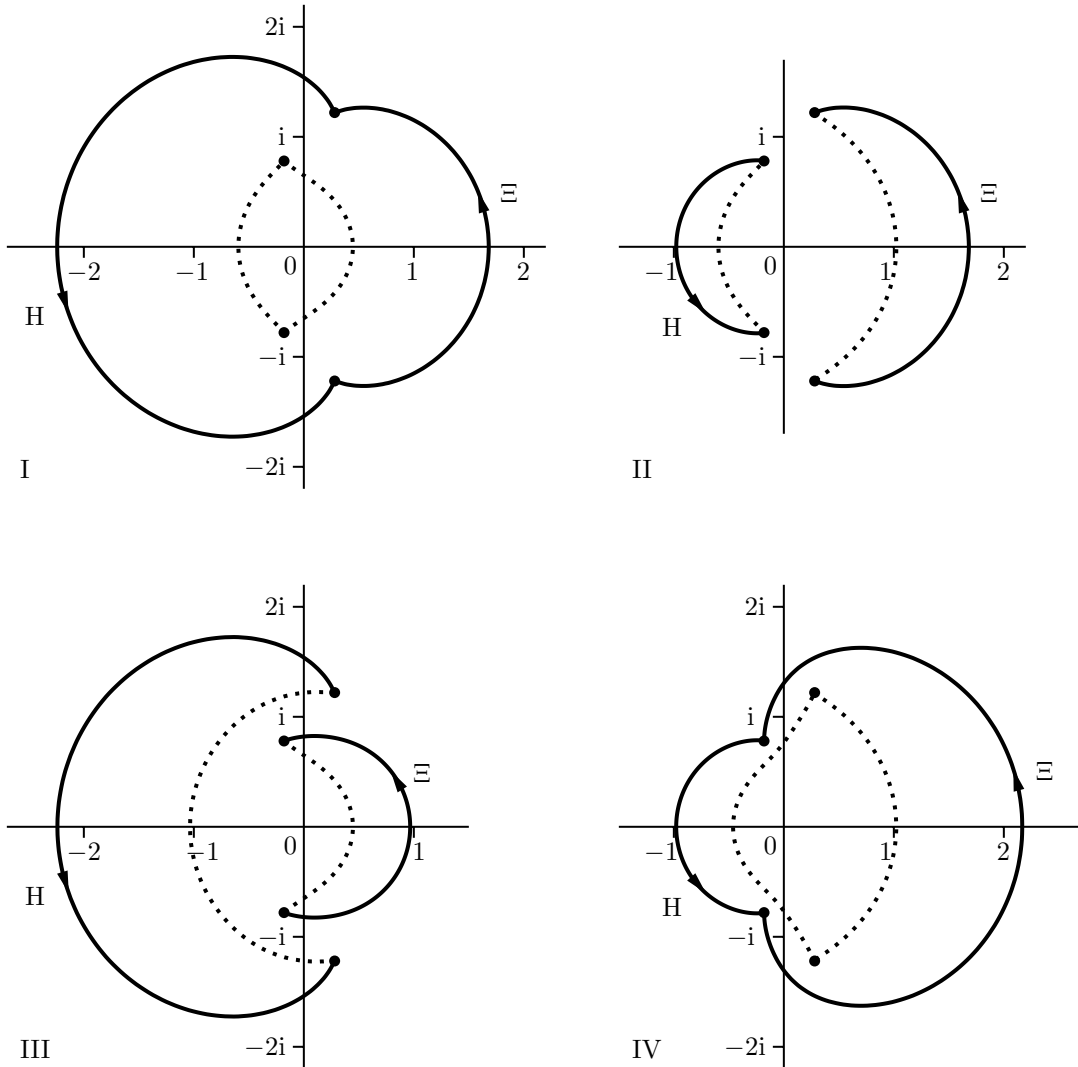


Figure 10: Four possible configurations of the curves Ξ and H . The dashed curved are $-\Xi^{-1}$ and $-H^{-1}$. In cases I and IV Ξ and H have the same end points. In cases II and III Ξ and $-H^{-1}$ share end points, as do H and $-\Xi^{-1}$.

The numerical results show that these four cases are related by the symmetries of the parameter space discussed in Subsection 4.2. They are in a single orbit of the sub-group of order six generated by the horizontal translation (which is of order three) and the product of the reflection in a

horizontal line and the reflection in a vertical line (which is of order two). For the remaining two members of this orbit we have not been able to numerically solve the BAEs. In these cases the particle densities are fairly high; we suppose that the curves Ξ and H would cross or otherwise violate the condition that $\hat{\Xi}$ and $\hat{\text{H}}$ only share their end points.

Once this symmetry is known a (numerical) calculation of the physical quantities needs to be carried out only for one of the four cases I–IV. The values for the other three cases are then obtained at once by application of the symmetry transformations.

6.4 Calculation of the sub-lattice densities and the entropy

In Subsection 6.1 the physical quantities ρ_L , ρ_R , ϕ_L , ϕ_R , and Φ pertaining to the semi-grand canonical ensemble were calculated from the functions $f_L(z)$ and $f_R(z)$. In Subsection 6.2 the derivatives $\frac{\partial\Phi}{\partial\phi_L}$ and $\frac{\partial\Phi}{\partial\phi_R}$ were computed. Substitution of these results into formulas (36)–(41) and (42) from Subsection 4.1 gives the sub-lattice densities and the entropy, physical quantities for the canonical ensemble. This was performed numerically for a particular value of \hat{b} . The results reveal that $\rho_0 = \rho_2 = \rho_4$ in cases I and IV and $\rho_1 = \rho_3 = \rho_5$ in cases II and III. From the expressions (36)–(41) for the sub-lattice densities this is equivalent to

$$\frac{\partial\Phi}{\partial\phi_L} = \frac{1}{6}(2 + \rho_L - 2\rho_R) \quad \text{and} \quad \frac{\partial\Phi}{\partial\phi_R} = \frac{1}{6}(2 - 2\rho_L + \rho_R) \quad (72)$$

in cases I and IV and

$$\frac{\partial\Phi}{\partial\phi_L} = \frac{1}{6}(-\rho_L + 2\rho_R) \quad \text{and} \quad \frac{\partial\Phi}{\partial\phi_R} = \frac{1}{6}(2\rho_L - \rho_R) \quad (73)$$

in cases II and III. One might hope to derive these expressions analytically from the results of Subsection 6.1–6.2. We have not tried this because it would involve rather cumbersome relations among integrals like (68), (69) and (70). Once the expressions (72) and (73) have been accepted the perturbation analysis approach from Subsection 6.2 becomes superfluous. Substituting them into (36)–(41) and (42) yields new expressions for the sub-lattice densities and the entropy. The expressions for the sub-lattice densities are polynomials in the particle densities ρ_L and ρ_R , the expression for the entropy also contains the phases ϕ_L and ϕ_R and of course the free energy Φ .

The cases I–IV correspond to different regions in the parameter space of sub-lattice densities, as given in Table 3. These four cases are defined for $\text{Re}\hat{b} > 0$ by Figure 10. The mirror images (with respect to the imaginary axis) of the configurations in Figure 10 define cases I'–IV' for $\text{Re}\hat{b} < 0$. For example, the locus of Ξ (H) for case I' is the mirror image of the locus of H (Ξ) for case I. Table 3 also lists the regions in the parameter space of sub-lattice densities corresponding to the cases I'–IV'.

Table 3: The regions in parameter space of the sub-lattice densities for the cases I–IV and I'–IV'.

$ b_L $	$ b_R $		$\text{Re}\hat{b} > 0$		$\text{Re}\hat{b} < 0$	
> 1	> 1	$\rho_0 = \rho_2 = \rho_4$	I	$\rho_1 > \rho_5 > \rho_3$	I'	$\rho_5 > \rho_1 > \rho_3$
> 1	< 1	$\rho_1 = \rho_3 = \rho_5$	II	$\rho_0 > \rho_2 > \rho_4$	III'	$\rho_4 > \rho_0 > \rho_2$
< 1	> 1	$\rho_1 = \rho_3 = \rho_5$	III	$\rho_2 > \rho_0 > \rho_4$	II'	$\rho_0 > \rho_4 > \rho_2$
< 1	< 1	$\rho_0 = \rho_2 = \rho_4$	IV	$\rho_5 > \rho_3 > \rho_1$	IV'	$\rho_1 > \rho_3 > \rho_5$

6.5 Summary

In the foregoing an exact solution of the trimer model was derived. Because the results are obtained in the course of a long derivation, we here provide a guide through them. The final result is the entropy as a function of six sub-lattice densities ρ_i defined in Subsection 2.1. Complete coverage of the lattice (1) and a further geometric constraint (2) (derived in Subsection 2.5) leave

four independent parameters. A full analytic solution in the thermodynamic limit is obtained in a two-parameter subspace.

The four-dimensional parameter space is described by new variables ρ_L , ρ_R , ϕ_L and ϕ_R . The free energy function of the ensemble with these parameters is denoted by Φ . The sub-lattice densities are expressed in ρ_L , ρ_R , $\frac{\partial\Phi}{\partial\phi_L}$ and $\frac{\partial\Phi}{\partial\phi_R}$ in (36)–(41); the entropy is given in terms of Φ , ϕ_L , ϕ_R , $\frac{\partial\Phi}{\partial\phi_L}$ and $\frac{\partial\Phi}{\partial\phi_R}$ in (42).

The free energy is written as a sum, $\Phi = -(\Sigma_L + \Sigma_R)$. In the solvable subspace the quantities ρ_L , ϕ_L and Σ_L are expressed as contour integrals of a function $f_L(z)$ in (68)–(70). Analogously the quantities ρ_R , ϕ_R and Σ_R are integrals of a function $f_R(z)$. The integration paths in the integral (68) for ρ_L and its analogue for ρ_R are contours Ξ and H , respectively. These contours are symmetric under complex conjugation. Their end points in the upper half plane are denoted b_L and b_R , respectively. These satisfy the equality $b_L - b_L^{-1} = b_R - b_R^{-1} = \hat{b}$. For each value of \hat{b} this equation has two distinct solutions for b_L and for b_R , resulting in four configurations I–IV of Ξ and H shown in Figure 10. The derivatives $\frac{\partial\Phi}{\partial\phi_L}$ and $\frac{\partial\Phi}{\partial\phi_R}$ are given by (72) in the cases I and IV and by (73) in the cases II and III.

The functions $f_L(z)$ and $f_R(z)$ are different branches of a function $f(z)$. The branch cuts of $f_L(z)$ are H and $-H^{-1}$, and $f_R(z)$ has branch cuts Ξ and $-\Xi^{-1}$. In terms of a new variable t , defined by (58) and (62), the function $f(z)$ is single-valued. It is given by (67), while the functions $f_L(z)$ and $f_R(z)$ are recovered by selecting the appropriate branch $t_L(z)$ and $t_R(z)$ of t , specified at the end of Subsection 5.4.

7 Phase diagram

In Subsections 2.1 and 2.5 a linear and a quadratic constraint on the six sub-lattice densities were derived. In this section we first show that these constraints imply a breaking of the symmetry between certain sub-lattices. This symmetry breaking suggests that a phase transition takes place when the total density $\rho_\nabla = \rho_1 + \rho_3 + \rho_5$ of down trimers is increased from 0 to 1. Next we compute the entropy as a function of ρ_∇ from the exact solution of this model. From this entropy the phase diagram of the model in the parameter ρ_∇ is obtained. It is also formulated in terms of the chemical potential of the down trimers instead of their density.

7.1 Symmetry breaking

The linear constraint (1) on the sub-lattice densities can be rewritten as

$$\rho_0 + \rho_2 + \rho_4 = 1 - \rho_\nabla, \quad (74)$$

and from the quadratic constraint (2) one has

$$\rho_0\rho_2 + \rho_2\rho_4 + \rho_4\rho_0 \leq \frac{1}{3}\rho_\nabla^2 \quad (75)$$

with equality if and only if $\rho_1 = \rho_3 = \rho_5 = \frac{1}{3}\rho_\nabla$. If ρ_∇ is small (to be precise: smaller than $2\sqrt{3} - 3$), it follows from (74) and (75) that one of ρ_0 , ρ_2 and ρ_4 is larger than the other two, say $\rho_0 > \rho_2, \rho_4$. Thus the symmetry between the sub-lattices 0, 2 and 4 is broken. If there is no further symmetry breaking then $\rho_2 = \rho_4$ and $\rho_1 = \rho_3 = \rho_5$, so

$$\rho_0 > \rho_1 = \rho_3 = \rho_5 > \rho_2 = \rho_4. \quad (76)$$

By the same token the symmetry between the sub-lattices 1, 3 and 5 is broken when ρ_∇ is close to 1. When ρ_∇ is increased from 0 to 1 the following seems to be the simplest possible scenario. At $\rho_\nabla = 0$ sub-lattice 0 is fully occupied and the other sub-lattices are empty. The six sub-lattice densities change continuously with ρ_∇ , and (76) holds up to $\rho_\nabla = \frac{1}{2}$. There the six sub-lattice densities are all equal to $\frac{1}{6}$. Then one of the odd sub-lattices, say 3, takes over, and

$$\rho_3 > \rho_0 = \rho_2 = \rho_4 > \rho_1 = \rho_5$$

all the way to $\rho_\nabla = 1$ where all trimers sit on sub-lattice 3.

7.2 Entropy for ρ_{∇}

In the previous subsection the occurrence was suggested of a phase transition when ρ_{∇} is increased from 0 to 1. For the study of such a phase transition it would be helpful to know the entropy of the model as a function of $\rho_{\nabla} = \rho_1 + \rho_3 + \rho_5$. However, what we have computed thus far is the entropy as a function of all sub-lattice densities, but only for a two-dimensional subspace. Therefore for given ρ_{∇} the sub-lattice densities have to be determined for which the entropy is maximal. If we are fortunate these sub-lattice densities happen to lie in the two-dimensional solved subspace.

For given $\rho_{\nabla} < \frac{1}{2}$ the most symmetric possibility for the six sub-lattice densities is described by (76). Another possibility,

$$\rho_2 = \rho_4 > \rho_1 = \rho_3 = \rho_5 > \rho_0, \quad (77)$$

exists when $2\sqrt{3} - 3 \leq \rho_{\nabla} < \frac{1}{2}$. Because of symmetry (76) and (77) are stationary points of the entropy. It is tempting to believe that (76), being the more general of the two most symmetric cases, corresponds to the maximum of the entropy. By numerically solving the BAEs the entropy of the model can be computed to high precision. Such calculations confirm that for $\rho_{\nabla} < \frac{1}{2}$ the entropy takes its maximum at the symmetric case (76) of the sub-lattice densities, hence within the solvable subspace.

As was seen in Subsection 6.4, for the solvable subspace one has $\rho_0 = \rho_2 = \rho_4$ in cases I and IV and $\rho_1 = \rho_3 = \rho_5$ in cases II and III. Consider case II and take \hat{b} on the imaginary axis between 0 and $2i$. The contours $\hat{\Xi}$ and \hat{H} then lie symmetric with respect to the imaginary axis, so $\rho_L = \rho_R$, and hence $\rho_2 = \rho_4$. Thus this is precisely the symmetric case (76). Therefore we have obtained the entropy as a function of ρ_{∇} for $\rho_{\nabla} < \frac{1}{2}$. The entropy for $\rho_{\nabla} > \frac{1}{2}$ follows immediately by the symmetry between up and down trimers. This entropy can also be obtained by considering case I and taking \hat{b} above $2i$ on the imaginary axis. The resulting entropy is shown in Figure 11. When in case II \hat{b} is not taken on the imaginary axis between 0 and $2i$, $\rho_2 \neq \rho_4$. Figure 12 shows the entropy as a function of the asymmetry $\rho_2 - \rho_4$ at fixed $\rho_1 = \rho_3 = \rho_5$ along the line determined by the constraints (1) and (2).

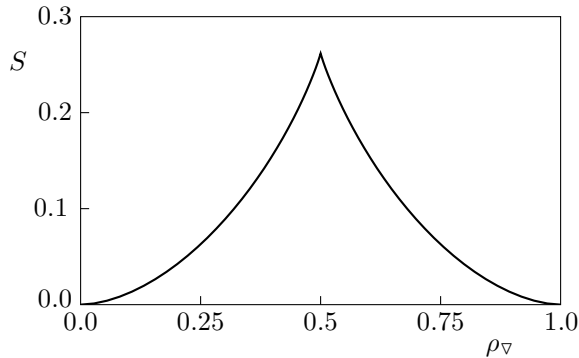


Figure 11: The entropy per trimer S as a function of the total density of down trimers $\rho_{\nabla} = \rho_1 + \rho_3 + \rho_5$. It is obtained from the exact solution in the special case (76) for $\rho_{\nabla} \leq \frac{1}{2}$, and similarly for $\rho_{\nabla} \geq \frac{1}{2}$.

For $\hat{b} = 2i$ all four cases I, II, III and IV coincide. The integrals in Subsection 6.1 then simplify. The sub-lattice densities are all equal to $\frac{1}{6}$, and the entropy per trimer is $S_{\text{sym}} = \log \frac{4}{3}\sqrt{3}$.

7.3 Phase transition

Consider a system with ρ_{∇} between 0 and $\frac{1}{2}$. The energy is a convex function of ρ_{∇} , so the system is thermodynamically unstable. It would separate into a frozen phase with $\rho_{\nabla} = 0$ and the

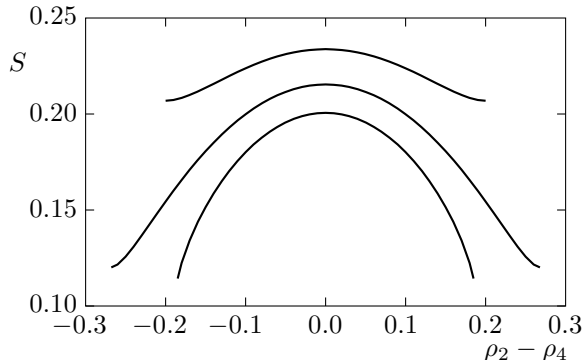


Figure 12: The entropy per trimer S as a function of $\rho_2 - \rho_4$ at fixed $\rho_1 = \rho_3 = \rho_5$. The end points of the lower curve ($\rho_\nabla = 0.45$) are determined by $\rho_2 = 0$ and by $\rho_4 = 0$. The upper curve ($\rho_\nabla = 0.48$) terminates when $\rho_4 = \rho_0$ and when $\rho_2 = \rho_0$. At the left end point of the middle curve ($\rho_\nabla = 2\sqrt{3} - 3 \approx 0.4641$) $\rho_2 = 0$ and $\rho_4 = \rho_0$, at the right end point $\rho_4 = 0$ and $\rho_2 = \rho_0$.

symmetric phase with $\rho_\nabla = \frac{1}{2}$. However an interface between these two phases is not possible in the model. Similarly a system with ρ_∇ between $\frac{1}{2}$ and 1 would demix into phases with $\rho_\nabla = \frac{1}{2}$ and $\rho_\nabla = 1$, if coexistence between these phases were possible.

Now give a chemical potential μ_∇ to the down trimers instead of imposing their density ρ_∇ . The free energy

$$F = -\mu_\nabla \rho_\nabla - S(\rho_\nabla)$$

takes its global minimum at

$$\rho_\nabla = \begin{cases} 0 & \text{for } \mu_\nabla \leq -2S_{\text{sym}} \\ \frac{1}{2} & \text{for } -2S_{\text{sym}} \leq \mu_\nabla \leq 2S_{\text{sym}} \\ 1 & \text{for } 2S_{\text{sym}} \leq \mu_\nabla \end{cases}$$

Therefore the model is in a frozen phase for $\mu_\nabla < -2S_{\text{sym}}$ and for $\mu_\nabla > 2S_{\text{sym}}$ and in the symmetric phase for $-2S_{\text{sym}} < \mu_\nabla < 2S_{\text{sym}}$. At $\mu_\nabla = -2S_{\text{sym}}$ and at $\mu_\nabla = 2S_{\text{sym}}$ there is coexistence between a frozen and a symmetric phase.

8 Conclusion

We have introduced a new simple lattice model. It is a fluid of particles each occupying three sites of the triangular lattice. We distinguish six sub-lattices of adsorption sites for the trimers. Full occupancy and a resulting geometric constraint leave of the six sub-lattice densities four independent parameters.

In the full four-dimensional parameter space the model is solvable by the Bethe Ansatz. In the thermodynamic limit the Bethe Ansatz equations can be reduced to two integral equations. In a two-dimensional subspace of the sub-lattice densities these integral equations can be solved by means of monodromy and analyticity properties of the functions involved. Within this subspace the entropy and the sub-lattice densities are given as integral expressions.

The solution is very similar to that of the square-triangle random tiling model [15,16]. In both cases the solution is closely connected to the hexagonal domain wall structure of the model. Another solvable model with such a domain wall structure is the three-colouring model on the honeycomb lattice [20]. In a configuration of this model the edges of the honeycomb lattice are coloured with three colours in such a way that the three edges meeting in each vertex have different colours. Alternatively this model can be formulated as the zero-temperature antiferromagnetic

three-state Potts model on the Kagomé lattice [21,22]. We shall now briefly discuss the relation between these three models.

The domain wall structure of the trimer model is depicted schematically in Figure 13. It contains two types of Y-joints but only one type of upside-down-Y-joints. In the square–triangle tiling there is only one type of Y-joints and one type of upside-down-Y-joints. In the honeycomb lattice three-colouring model on the other hand both the Y-joints and the upside-down-Y-joints come in two types. Hence these three models appear to be different.

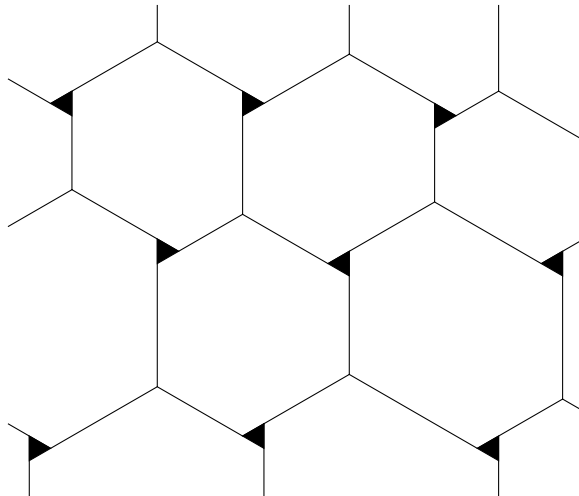


Figure 13: Schematic representation of the domain wall structure of the trimer model. The Y-joints of the domain walls come in two types. These are mirror images, featuring either a ◀ or a ▶. In contrast there is only one type of upside-down-Y-joints.

The $A_2^{(1)}$ model is a vertex model on the square lattice, derived from an affine Lie algebra [23,24]. It satisfies the Yang–Baxter equation [25,26], so it can be solved by algebraic Bethe Ansatz [27]. At a special value of the spectral parameter it is the three-colouring model on the honeycomb-lattice [28]. For a suitable choice of the remaining parameters one of the two types of Y-joints and upside-down-Y-joints in the domain wall network is excluded. In this limit the model is just the square–triangle tiling. This mapping “explains” the solvability of the square–triangle tiling in terms of that of the $A_2^{(1)}$ model [29].

In a similar fashion the square–triangle tiling can also be obtained from the trimer model. When the trimers on sub-lattice 4 (or 2) are excluded, one (or the other) type of Y-joint no longer occurs in the domain wall network. Again the square–triangle tiling results. The Bethe Ansatz for the trimer model remains valid in this special case. However, the substitutions (26) no longer makes sense when $w_4 = 0$ (or $w_2 = 0$), so the same is true of the analysis in the subsequent sections.

Therefore the three models are connected in sense that both the trimer model and the $A_2^{(1)}$ model contain the square–triangle random tiling as a singular limit. It would be interesting to know if the trimer model, like the square–triangle tiling, is a special case of some model satisfying the Yang–Baxter equation.

Acknowledgement

We are grateful to Jan de Gier for many useful discussions, as well as for putting at our disposal his computer program for numerical Bethe Ansatz calculations. We thank Dave Rusin for enlightening us on the question whether the integrals from Subsection 6.1 can be expressed in closed form. This

work is part of the research programme of the “Stichting voor Fundamenteel Onderzoek der Materie (FOM)”, which is financially supported by the “Nederlandse Organisatie voor Wetenschappelijk Onderzoek (NWO)”.

A Perturbation analysis

In Subsection 6.1 the quantities $\rho_L, \rho_R, \phi_L, \phi_R$ and $\Phi = -(\Sigma_L + \Sigma_R)$ were obtained as functions of $\hat{b} = \hat{b}_L = \hat{b}_R$. For the computation of the sub-lattice densities and the entropy the derivatives

$$\left(\frac{\partial \Phi}{\partial \phi_L} \right)_{\rho_L \rho_R \phi_R} \quad \text{and} \quad \left(\frac{\partial \Phi}{\partial \phi_R} \right)_{\rho_L \rho_R \phi_L}$$

are also needed as functions of \hat{b} . These cannot be calculated by differentiation of the Φ already obtained, because variation of ϕ_L (ϕ_R) at constant ρ_L, ρ_R and ϕ_R (ϕ_L) breaks the condition $\hat{b}_L = \hat{b}_R$. Therefore in this appendix we infinitesimally relax that condition, and compute $\rho_L, \rho_R, \phi_L, \phi_R$ and $\Phi = -(\Sigma_L + \Sigma_R)$ to leading order in the infinitesimal relaxation parameter.

When the curves $\hat{\Xi}$ and \hat{H} do not close, the monodromy group is the full group $\text{SL}(2, \mathbf{Z})$. Therefore $g_L(\hat{z})$ and $g_R(\hat{z})$ are no longer single-valued functions of the variable t . Kalugin [16] has provided a perturbation analysis for the analogous situation in the square–triangle random tiling model. It leans heavily on the understanding of the structure of the Riemann surface of the functions. Our approach does not require such knowledge and is more systematic.

Although $g_L(\hat{z})$ and $g_R(\hat{z})$ are no longer single-valued functions of the variable t , one can still perform the variable transformation (62). The end points \hat{b}_L and \hat{b}_L^* of $\hat{\Xi}$ (\hat{b}_R and \hat{b}_R^* of \hat{H}) then correspond to points d_L and d_L^{*-1} (d_R and d_R^{*-1}) in the t -plane. The point \hat{b} in (62) can be chosen such that $|d_L| = |d_R|$; write

$$d_L = \beta_L \delta \quad \text{and} \quad d_R = \beta_R \delta,$$

with δ real and positive and $|\beta_L| = |\beta_R| = 1$. The curves corresponding to $\hat{\Xi}$ and \hat{H} divide the annulus $\delta < |t| < \delta^{-1}$ into sectors, much as in Figure 9. We get a single-valued function $h(t) = g(\hat{z})$ in this annulus instead of in the whole t -plane. Since it is analytic in the annulus it can be expanded as a Laurent series in t :

$$g(\hat{z}) = h(t) = \sum_{p=-\infty}^{\infty} A_p t^p. \quad (78)$$

Only powers t^p with $p \equiv \pm 1 \pmod{6}$ have the correct monodromy properties, so other powers cannot occur. From (50) one has

$$h(t^{*-1}) = g(\hat{z}^*) = g(\hat{z})^* = h(t)^*,$$

so the coefficients A_p satisfy

$$A_{-p} = A_p^*. \quad (79)$$

We want to view the function $g(\hat{z})$ given by (78) as a perturbation of the function $g(\hat{z})$ given by (66), where δ is the small parameter. In our notation we have suppressed the dependence of the coefficients A_p on δ, β_L , and β_R .

The function $g(\hat{z})$ satisfies the integral equation (60). We investigate how each of the terms t^p from the Laurent series (78) of $g(\hat{z})$ behaves in this equation. In order to compute the integral we change from $\hat{\eta}$ to $\tau = t(\hat{\eta})$ as integration variable. The resulting integrand is a rational function in τ , which we decompose into partial fractions. Integration yields polynomial as well as logarithmic

terms; some care is required in choosing the branch of the logarithms. Finally we expand in powers of δ , obtaining

$$\frac{1}{2\pi i} \int_{\hat{\mathbb{H}}} \frac{1}{\hat{\eta} - \hat{z}} \tau^p d\hat{\eta} = t^p - t_1^p + \frac{6}{2\pi i} \left\{ \sum_{q=-\infty}^{-1} \frac{\beta_{\mathbb{R}}^{p-6q}}{p-6q} (t^{6q} - 1) \delta^{p-6q} + \sum_{q=1}^{\infty} \frac{\beta_{\mathbb{R}}^{p-6q}}{p-6q} (t^{6q} - 1) \delta^{6q-p} \right\} \quad (80)$$

for each term t^p in the Laurent series (78). Here t in the RHS corresponding to \hat{z} in the LHS is in the sector containing t_1 , that is the sector where $g(\hat{z})$ equals $g_{\mathbb{L}}(\hat{z})$. Comparison with the integral equation (60) shows the following. The term t^p in the RHS of (80) exactly matches the term $g_{\mathbb{L}}(\hat{z})$ in the LHS of (60). The inhomogeneous term $-t_1^p$ in the RHS of (80) corresponds to the inhomogeneous term 1 in the integral equation. The other terms in the RHS of (80) are “unwanted”; the powers of t they involve are multiples of 6. Because the Laurent series (78) satisfies the integral equation (60) the inhomogeneous terms $-t_1^p$ from (80) counterbalance the inhomogeneous term 1 of the integral equation,

$$\sum_{p=-\infty}^{\infty} t_1^p A_p = 1 \quad (81)$$

(which means that $g_{\mathbb{L}}(\infty) = 1$), and the unwanted terms cancel,

$$\sum_{p=-\infty}^{\infty} \frac{\beta_{\mathbb{R}}^p}{p-6q} \delta^p A_p = 0 \quad \text{for all } q < 0, \quad (82)$$

$$\sum_{p=-\infty}^{\infty} \frac{\beta_{\mathbb{R}}^p}{p-6q} \delta^{-p} A_p = 0 \quad \text{for all } q > 0. \quad (83)$$

(Due to (79) the equations for q and for $-q$ are equivalent.) The function $g(\hat{z})$ also satisfies the integral equation (61); this leads to another similar set of conditions on the coefficients A_p .

The form of the equations (82) and (83) and their analogue from (61) suggests that for $\beta_{\mathbb{L}}$ and $\beta_{\mathbb{R}}$ fixed the coefficients A_p should be power series in δ ,

$$A_p = A_p^{(0)} + A_p^{(1)}\delta + A_p^{(2)}\delta^2 + \dots \quad (84)$$

We would like to determine the coefficients $A_p^{(h)}$.

When t approaches the boundary of the annulus, $|t| \rightarrow \delta$ or $|t| \rightarrow \delta^{-1}$, the unperturbed function $g(\hat{z})$ given by (66) becomes of the order δ . It seems reasonable to assume that the terms $A_p t^p$ of the perturbed function $g(\hat{z})$ do not grow faster than this, so the coefficients $A_p^{(h)}$ with $h < |p| - 1$ must be zero.

Consider (81) and its analogue from (61). Substitution of the power series (84) yields, after rearrangement of the terms,

$$\sum_{h=0}^{\infty} \delta^h \left(\sum_{p=-(h+1)}^{h+1} t_k^p A_p^{(h)} \right) = 1 \quad \text{for } k = 1, 5. \quad (85)$$

The δ^0 part gives

$$t_k A_1^{(0)} + t_k^{-1} A_{-1}^{(0)} = 1 \quad \text{for } k = 1, 5.$$

The unique solution of these equations reproduces the unperturbed function $g(\hat{z})$ given by (66). For $1 \leq h \leq 3$ the δ^h part of (85) gives

$$t_k A_1^{(h)} + t_k^{-1} A_{-1}^{(h)} = 0 \quad \text{for } k = 1, 5.$$

This implies that $A_1^{(h)}$ and $A_{-1}^{(h)}$ are zero. The δ^4 part of (85) gives

$$t_k A_1^{(4)} + t_k^{-1} A_{-1}^{(4)} + t_k^5 A_5^{(4)} + t_k^{-5} A_{-5}^{(4)} = 0 \quad \text{for} \quad k = 1, 5.$$

These equations have two linearly independent solutions, one of which satisfies (79). Substituting these results into (84) and (78) yields

$$g(\hat{z}) = t + t^{-1} + C(t^{-5} - t) + C^*(t^5 - t^{-1}) + O(\delta^5), \quad (86)$$

where we have written

$$A_{-5}^{(4)} \delta^4 = C \quad \text{and} \quad A_5^{(4)} \delta^4 = C^*.$$

Note that (86) can be written in the form (64). We have used the equations (82) and (83) only to come up with the series expansion (84). These equations would be needed if the coefficients $A_p^{(h)}$ with $h > 4$ were to be determined. Knowledge of these coefficients would yield a solution to the integral equations (60) and (61) also for a finite opening between \hat{b}_L and \hat{b}_R . Unfortunately we have not been able to calculate these coefficients, but fortunately they are not needed, because the present purpose is only to compute ρ_L , ρ_R , ϕ_L , ϕ_R and $\Phi = -(\Sigma_L + \Sigma_R)$ only to leading order in δ .

As our aim is to calculate the quantities ρ_L , ρ_R , ϕ_L , ϕ_R and Φ , we substitute (78) and (84) into the integral expressions from Subsection 6.1. For (68) this gives, after transforming to t as integration variable:

$$\rho_L = \frac{1}{2\pi i} \sum_{p=-\infty}^{\infty} \sum_{h=|p|-1}^{\infty} A_p^{(h)} \delta^h \int_{\beta_L \delta^{-1}}^{\beta_L \delta} t^p \frac{1}{\sqrt{\hat{z}^2 + 4}} \frac{d\hat{z}}{dt} dt. \quad (87)$$

For each p and h we determine the order in δ of the contribution. When $t \rightarrow 0$ or $t \rightarrow \infty$ the integrand is proportional to t^{p+5} and t^{p-7} , respectively. Hence the integral is bounded, of order 0 in δ that is, for $|p| \leq 5$; logarithmic in δ for $|p| = 6$; of order $6 - |p|$ in δ for $|p| \geq 7$. Note that the coefficients $A_p^{(h)}$ with $|p| = 6$ are zero. Let m denote the order in δ of the integral. The order in δ of the whole contribution is $h + m$:

$ p $	m	h	$h + m$
1	0	0	0
1	0	4	4
1	0	≥ 5	≥ 5
5	0	4	4
5	0	≥ 5	≥ 5
≥ 7	$6 - p $	$\geq p - 1$	≥ 5

Therefore ρ_L in (87) has a δ^0 contribution from the unperturbed part in the RHS of (86), a δ^4 contribution from the part involving C and C^* , and contributions of higher order in δ from the parts collected in the $O(\delta^5)$ term, so

$$\rho_L = \frac{1}{2\pi i} \int_{\beta_L \delta^{-1}}^{\beta_L \delta} [t + t^{-1} + C(t^{-5} - t) + C^*(t^5 - t^{-1})] \frac{1}{\sqrt{\hat{z}^2 + 4}} \frac{d\hat{z}}{dt} dt + O(\delta^5).$$

In the RHS the integration limits may be changed from $\beta_L \delta^{-1}$ and $\beta_L \delta$ to ∞ and 0, as this makes a difference $O(\delta^5)$. Transforming back to z as integration variable then gives

$$\rho_L = \frac{1}{2\pi i} \int_{\Xi^{(0)}} [t + t^{-1} + C(t^{-5} - t) + C^*(t^5 - t^{-1})] dz + O(\delta^5),$$

where $\Xi^{(0)}$ denotes the unperturbed ($\delta = 0$) contour. Hence ρ_L is given to leading order in $C \sim \delta^4$ by (68), where now $f(z)$ is given by (71) instead of (67), and integration is over the unperturbed

contour. Note that β_L and β_R do not occur in this expression. Similar arguments show that fully analogous results hold for ρ_R , ϕ_L , ϕ_R , Σ_L and Σ_R : up to $O(\delta^5)$ they are given by the integrals (68), (69) and (70) or their R-analogues, with $f(z)$ given by (71). Therefore we have now obtained these quantities to leading order, namely δ^4 , in the parameter δ that describes the infinitesimally small opening $\hat{b}_L - \hat{b}_R \sim \delta^6$ between the end points of $\hat{\Xi}$ and \hat{H} .

References

- [1] R. H. Fowler and G. S. Rushbrooke, *Trans. Faraday Soc.* **33**, 1272 (1937).
- [2] P. W. Kasteleyn, *Physica* **27**, 1209 (1961).
- [3] H. N. V. Temperley and M. E. Fisher, *Phil. Mag. [8th Ser.]* **6**, 1061 (1961).
- [4] E. H. Lieb, *Phys. Rev. Lett.* **18**, 692 (1967).
- [5] E. H. Lieb, *Phys. Rev.* **162**, 162 (1967).
- [6] E. H. Lieb, *Phys. Rev. Lett.* **18**, 1046 (1967).
- [7] E. H. Lieb, *Phys. Rev. Lett.* **19**, 108 (1967).
- [8] B. Sutherland, *Phys. Rev. Lett.* **19**, 103 (1967).
- [9] C. P. Yang, *Phys. Rev. Lett.* **19**, 586 (1967).
- [10] B. Sutherland, C. N. Yang, and C. P. Yang, *Phys. Rev. Lett.* **19**, 588 (1967).
- [11] E. H. Lieb and F. Y. Wu, Two-dimensional ferroelectric models, in *Phase Transitions and Critical Phenomena*, edited by C. Domb and M. S. Green, volume 1, pages 321–490, Academic Press, London, 1972.
- [12] J. F. Nagle, C. S. O. Yokoi, and S. M. Bhattacharjee, Dimer models on anisotropic lattices, in *Phase Transitions and Critical Phenomena*, edited by C. Domb and J. L. Lebowitz, volume 13, pages 235–297, Academic Press, London, 1989.
- [13] J. Villain, Two-dimensional solids and their interactions with substrates, in *Ordering in Strongly Fluctuating Condensed Matter Systems*, edited by T. Riste, pages 221–253, Plenum Press, New York, 1980.
- [14] H. Kawamura, *Prog. Theor. Phys.* **70**, 352 (1983).
- [15] M. Widom, *Phys. Rev. Lett.* **70**, 2094 (1993).
- [16] P. A. Kalugin, *J. Phys. A: Math. Gen.* **27**, 3599 (1994).
- [17] A. Verberkmoes and B. Nienhuis, *cond-mat/9904343*.
- [18] J. de Gier and B. Nienhuis, *J. Stat. Phys.* **87**, 415 (1997).
- [19] J. de Gier and B. Nienhuis, *J. Phys. A: Math. Gen.* **31**, 2141 (1998).
- [20] R. J. Baxter, *J. Math. Phys.* **11**, 784 (1970).
- [21] F. Y. Wu, *Rev. Mod. Phys.* **54**, 235 (1982).
- [22] D. A. Huse and A. D. Rutenberg, *Phys. Rev. B* **45**, 7536 (1992).
- [23] V. V. Bazhanov, *Phys. Lett.* **159B**, 321 (1985).
- [24] M. Jimbo, *Commun. Math. Phys.* **102**, 537 (1986).

- [25] R. J. Baxter, *Ann. Phys. (N.Y.)* **70**, 193 (1972).
- [26] R. J. Baxter, *Exactly Solved Models in Statistical Mechanics*, Academic Press, London, 1982.
- [27] L. D. Faddeev and L. A. Takhtadzhyan, *J. Sov. Math.* **24**, 241 (1984).
- [28] N. Y. Reshetikhin, *J. Phys. A: Math. Gen.* **24**, 2387 (1991).
- [29] J. de Gier and B. Nienhuis, *Phys. Rev. E* **55**, 3926 (1997).